# Performance evaluation of solar heat systems integrated with seasonal heat storage across varied operating modes for building applications

## The case of Netherlands

Ul-Abdin, Zain; Isabella, Olindo; Santbergen, Rudi

**DOI**
10.1016/j.solener.2025.113772

**Publication date**
2025

**Document Version**
Final published version

**Published in**
Solar Energy

Solar Energy 299 (2025) 113772

Contents lists available at ScienceDirect

Solar Energy

journal homepage: www.elsevier.com/locate/solener

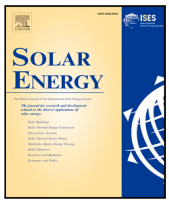

# Performance evaluation of solar heat systems integrated with seasonal heat storage across varied operating modes for building applications: The case of Netherlands

Zain Ul-Abdin *, Olindo Isabella, Rudi Santbergen

*Photovoltaic Materials and Devices Group, Delft University of Technology, Mekelweg 4, Delft, 2628 CD, The Netherlands*

ARTICLE INFO

*Keywords:*
PV(thermal) collectors
Thermal heat storage
Heat pump
Operating modes
Energy demand
Building performance

ABSTRACT

In this study, a modeling methodology is presented for evaluating the performance of a hybrid system integrating different types of solar collectors, namely photovoltaic (PV), glazed flat plate solar thermal (ST) and unglazed photovoltaic-thermal (PVT) collectors to harvest solar energy. Further, the system is integrated with a seasonal storage that is an aquifer thermal energy storage (ATES) system, a heat exchanger and a heat pump (HP) to provide heating, including space heating (SH), domestic hot water (DHW), as well as cooling. The investigation considers various operational modes depending on the climate conditions and building characteristics. The study focuses on comparison of solar collectors in realistic scenarios, examining heating type and insulation levels. Real energy consumption data considering five residential buildings in Amsterdam is employed for the analysis. Annual simulations for the considered buildings are conducted for SH and DHW coverage, along with cooling. The results indicate that ATES combined with glazed ST collectors demonstrates superior heat storage while HP with PV/ST combination and floor heating achieves an average coefficient of performance (COP) of 6.09 for both SH and DHW. In contrast, HP combined with PVTs shows the lowest performance, with a COP of around 5 when used with radiator heating. Additionally, majority of the demand is covered using HP storage mode with seasonal storage and HP while building insulation plays a crucial role.

## 1. Introduction

Fossil fuels have long dominated global energy landscape [1], but this is now changing. In 2024, the European Union's energy transition accelerated as the amount of solar energy surpassed the energy from coal for the first time [2], a crucial step in reducing carbon footprint. The building sector plays a significant role in the total energy consumption. It accounts for about 40% of the global energy consumption [3,4]. The major energy use is associated with lighting, ventilation, space heating/cooling, and domestic water heating. Reducing energy consumption in buildings is crucial in combating global warming and supporting low-carbon communities [5]. Researchers are increasingly investigating renewable energy systems to boost their economic viability. They aim to stabilize the greenhouse gas concentrations in the atmosphere and avoid disastrous climate change consequences [6]. Solar energy, as a readily accessible renewable resource, is accessible in both direct and indirect forms [7]. Solar systems can be classified into two main categories: solar thermal (ST) and photovoltaic (PV) modules, each operating on distinct principles. Solar PV technology is widely used way to generate electricity [8]. On the other hand, ST collector is the most common solar technology for heating applications [9]. PV–thermal (PVT) collectors integrate the two technologies ST and PV [10], allowing for simultaneous production of electricity and hot water (warm air in case of an air-based collector). This integration enables more efficient use of solar resources and roof space [11]. These collectors can achieve higher overall avoided primary energy compared to only PV and ST modules, as they utilize less space, making them suitable for applications with limited space [12]. The cooling effect of circulating water in PVT systems can enhance the efficiency of PV panels, leading to improved electricity generation.

In some countries, like the Netherlands, there is so much PV installed, 1500 Wp per capita, that during sunny times, electricity supply exceeds demand, and PV modules have to be shut off. This highlights the issue of grid congestion, driven by two factors: excess PV feed-in during sunny periods, and increased electricity demand from the electrification of heating systems [13]. The excess electricity generated by PV modules during peak sunlight hours can be utilized to power heat pumps (HPs). The mainstream HP technologies are categorized into air source HP, water source HP, and ground source HP, depending on the

* Corresponding author.
*E-mail address:* z.ulabdin@tudelft.nl (Z. Ul-Abdin).

https://doi.org/10.1016/j.solener.2025.113772
Received 17 February 2025; Received in revised form 7 June 2025; Accepted 6 July 2025
Available online 21 July 2025

## Nomenclature

### Abbreviations

| | |
|---|---|
| $ATES$ | Aquifer thermal energy storage |
| $COP$ | Coefficient of performance |
| $DHW$ | Domestic hot water |
| $HP$ | Heat pump |
| $PV$ | Photovoltaic |
| $PVT$ | PV–thermal |
| $SH$ | Space heating |
| $ST$ | Solar thermal |

### Symbols

| | |
|---|---|
| $A$ | Area ($m^2$) |
| $C$ | Specific heat capacity (J $kg^{-1}$ $K^{-1}$) |
| $E$ | Energy (Wh) |
| $\mathscr{E}$ | Exergy (W) |
| $G$ | Solar irradiance (W $m^{-2}$) |
| $H$ | Enthalpy (J $kg^{-1}$) |
| $h$ | Heat transfer coefficient (W $m^{-2}$ $K^{-1}$) |
| $k$ | Conductivity (W $m^{-1}$ $K^{-1}$) |
| $\ell$ | Thickness of a component (m) |
| $L$ | Length of the module (m) |
| $\dot{m}$ | Mass flow rate (kg $s^{-1}$) |
| $M$ | Mass (kg) |
| $n$ | Porosity |
| $P$ | Pressure (Pa) |
| $\mathscr{P}$ | Power (W) |
| $T$ | Temperature (K) |
| $V$ | Volume ($m^3$) |
| $V_w$ | Wind speed (m $s^{-1}$) |
| $W$ | Width of the module (m) |

### Greek letters

| | |
|---|---|
| $\alpha$ | Absorptance |
| $\beta$ | Thermal expansion coefficient, 1/T ($K^{-1}$) |
| $\beta_p$ | Temperature coefficient of maximum power, $K^{-1}$ |
| $\delta$ | Solar radiation coefficient |
| $\varepsilon$ | Emissivity |
| $\eta$ | Efficiency |
| $\lambda$ | Thermal conductivity (W $m^{-1}$ $K^{-1}$) |
| $\rho$ | Density (kg $m^{-3}$) |
| $\tau$ | Transmissivity |

### Subscripts & Superscripts

| | |
|---|---|
| $ab$ | Absorber |
| $am$ | Ambient |
| $aq$ | Aquifer |
| $aqt$ | Aquitard |
| $c$ | Conductive |
| $cf$ | Confined air space |
| $el$ | Electrical |
| $g$ | Glass |
| $h, aq$ | Horizontal hydraulic aquifer |
| $h, aqt$ | Horizontal hydraulic aquitard |
| $i$ | Insulator |
| $m$ | Metallic tube |
| $mod$ | Module |
| $pv$ | PV cell |
| $r$ | Radiative |
| $ref$ | Reference |
| $sc$ | Sand and clay |
| $s$ | Sky |
| $t$ | Tedlar |
| $th$ | Thermal |
| $v$ | Convective |
| $v, aq$ | Vertical hydraulic aquifer |
| $v, aqt$ | Vertical hydraulic aquitard |
| $w$ | Water fluid |

type of heat source [14]. Moreover, heat storage is considered as an important way in decarbonizing building energy sectors, particularly in scenarios where heating demand does not synchronize with solar energy potential availability. PV(T) collectors combined with a HP and a heat storage is a promising solution. The surplus thermal energy generated by ST and PVT collectors during sunny periods can be efficiently stored in the underground aquifer using seasonal aquifer thermal energy storage (ATES) technology. During times of high energy demand or when solar energy availability is low, the stored thermal energy can be extracted from the aquifer and utilized for space heating (SH), domestic hot water (DHW) production, or other heating applications. ATES seasonal storage systems possess global potential to offer environmentally friendly SH, DHW and cooling for buildings. The system utilizes underground water-bearing layers, known as aquifers, to store either hot or cold fluid. A typical ATES comprises multiple cold and warm aquifers [15]. The groundwater is used as a working fluid which is injected and extracted from the aquifer to store and extract the thermal energy. The temperature of the warm water injected by the warm well is typically 15 to 18 °C, while the temperature of the cold water injected by the cold well is 5 to 10 °C. Considering the natural temperature is approximately 12 °C, this reflects a temperature difference of around 5 °C for both heating and cooling processes [16]. Geological conditions and system design govern the efficiency of such a system since they impact the thermal recovery efficiency and energy conservation in these aquifers. The success of an ATES system depends on its thermal recovery efficiency. It is the ratio of recovered energy to injected energy, influencing both its technical and economic performance [17].

Studies performed by [18–20] have explored various thermal energy storage strategies integrated with PV systems for residential heating applications. While these studies contribute valuable insights into short-term and latent thermal energy storage, they do not address seasonal storage for year-round applications. Zhang et al. [21] compared and analyzed various solar utilization schemes (PV, ST and PVT) alongside different parameters (load and available roof area). Results showed that PVT yields 8.20% higher electrical energy output than PV alone. Additionally, PV module combined with a PVT scheme exhibits the best economic performance among the four schemes examined. However, gas boilers and auxiliary electrical heaters are employed in this study. The performance of PV, PVT, and solar domestic water heating systems was assessed in Morocco's climate by Seddik et al. [6]. Integrating the thermal part with the heat storage tank, which is not seasonal, limits performance on cloudy days. Results show PVT system's annual mean thermal and electrical exergy efficiency is 12%, higher than PV (11%) and domestic water heater (3%) systems. A PVT air source HP system has been installed by Triple Solar, with ongoing

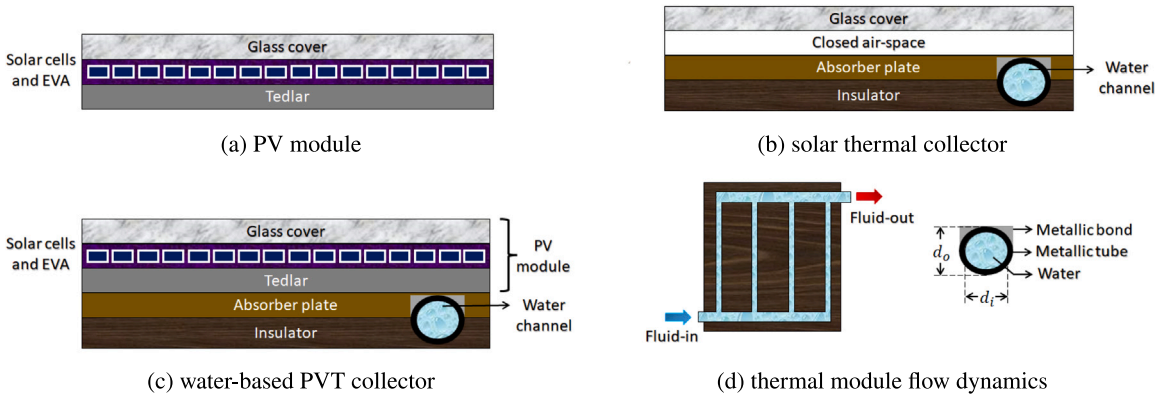


**Fig. 1.** Schematic cross-sectional view of (a) photovoltaic module, (b) solar thermal collector, (c) water-based photovoltaic thermal collector, and (d) thermal module flow dynamics.

experiments, to create an affordable home setup at the Green Village at TU Delft [22]. Del Amo et al. [23] proposed a simple model for a solar-assisted HP integrating PVT panels. The study recommends incorporating seasonal storage to harness excess heat generated during summer, maximizing efficiency. Clauß and Georges [24] investigated the impact of modeling complexity on a HP. The heat pump directly heats the domestic storage tank, while a ST collector, integrated via a heat exchanger, supplements DHW provision. It was found that a perfectly modulating HP, which continuously adjusts its output to maintain optimal tank temperature, made the system perform better than expected. Combining ground source HP systems with PVT relies mainly on boreholes, necessitating extensive installation space and drilling expenses. Nevertheless, the integration of ground source HP has minimal impact on PVT cell performance [25]. However, solar energy systems with both HP and seasonal storage have not been studied in detail. A multi-energy system model was developed by Perera et al. [26], incorporating electrical and seasonal thermal storage, with a boiler for the thermal aspect and PV panels for the electrical aspect. The study found that adopting ATES can enhance renewable energy penetration and reduce reliance on fossil fuels, with grid and HP support. Ghaebi et al. [27] conducted a numerical simulation using the finite difference method, coupling ATES with the HP and a flat plate ST collector. Only two operating modes for ATES were considered: cyclic, where wells switch seasonally, and continuous, where wells remain unchanged. Results showed that coupling ATES with the HP achieved a COP of 17.2 for cooling and around 5 for heating. Combining ATES with a flat plate ST collector for heating only yielded a COP of 19.6. Fleuchaus et al. [28] analyzed 73 Dutch ATES systems to evaluate their technical performance. Results indicate that, on average, the temperatures at which water is extracted from the aquifer are 10 °C in summer and 15 °C in winter, with temperature losses during storage ranging between 1 and 2 °C.

This study integrates various elements, such as solar collectors, a HP, and a low temperature ATES system (seasonal storage), while exploring diverse operational modes for SH, DHW, and cooling. This integrated combination not only enhances performance but also contributes to lower operating costs and reduced carbon emissions, making it a promising solution for sustainable heating and cooling applications. ATES is chosen in this study as it is particularly well-suited to the Dutch context. Recent research conducted by Deltares [29] shows that the Netherlands offers ideal conditions for ATES, making it a highly effective storage solution. Many studies in literature predict thermal module temperatures using quasi-steady approaches, assuming steady-state operation. While some studies incorporate dynamic response, they mainly focus on daily simulations. This study distinguishes itself from previous research by introducing dynamic thermal models to estimate temperature distribution and achieve realistic annual performance, thermal and electrical. By incorporating annual simulations based on real weather data, it ensures a more accurate prediction of system performance throughout the entire year. Additionally, two SH cases were considered: radiator heating and floor heating. The integration offers a significant step towards optimizing the efficiency and sustainability of energy systems. In previous studies, challenges like excess heat production during periods of high solar radiation or low heat demand are encountered. To optimize their efficiency and lifespan, effective seasonal storage solution for surplus heat combined with the HP is developed. This solution is critical for maximizing system energy output, improving performance, and accelerating the shift towards cleaner, sustainable energy sources. The effect of the occupants on the energy demand is neglected in the literature. In this study, this parameter is taken into account, further enhancing the real-world applicability of the results. The developed models are further incorporated into the Photovoltaic Materials and Devices (PVMD) toolbox [30], which can already predict the energy yield of PV systems and air-based PVT collectors. It can also predict a novel bi-fluid-based PVT system embedded with a short-term heat storage solution [31], expanding its functionality. To the best of our knowledge, this integration, combining two solar collectors, floor and radiator heating, multiple modes for SH, DHW, and cooling under realistic building conditions, has not been discussed in the literature. The objective is to assess and compare the annual and weekly performance of different configurations to identify the most effective solution for meeting energy demands of buildings in the Amsterdam region. This work is significant as it lays the groundwork for more efficient, adaptable, and sustainable heating and cooling solutions that can be scaled to various urban contexts.

The subsequent sections of this paper are organized as follows: Section 2 introduces the numerical models of various solar collectors (including PV module, ST collector and PVT collector), as well as a HP and an ATES system. In Section 3, the comprehensive integration of all system components, along with various heating and cooling modes, is discussed. Section 4 describes the input parameters, including demand side inputs and weather data. This is followed by Section 5, which details the results and discussion. Finally, the paper ends with a conclusion and some perspectives.

## 2. Modeling of the system

This section outlines and discusses various solar collectors with an area of approximately 2 $m^2$ per module, oriented to the south with a tilt angle of 31°. It also covers seasonal thermal storage (ATES) and a heat pump. The ATES system having two aquifers is coupled with a water source HP, an important component facilitating the exchange of thermal energy, thereby enhancing performance of the system. Moreover, a heat exchanger is incorporated for the transfer of heat. The details are presented in the subsequent sections.

### 2.1. Photovoltaic module

A PV module illustrated in Fig. 1(a) consists of three main components: a glass cover, a layer of solar PV cells embedded in ethylene vinyl acetate (EVA) and a protective tedlar layer beneath the cells. The aim is to derive a set of equations that predict the behavior of the solar collector. The heat balance equation for each element within the PV module (i.e. glass, PV cell and tedlar) can be expressed as:

$$\begin{cases} M_g C_g \dfrac{dT_g}{dt} = A_{mod}[\alpha_g G - h_r^{g-s}(T_g - T_s) - h_v^{am}(T_g - T_{am}) \\ \quad - h_c^{g-pv}(T_g - T_{pv})] \\ M_{pv} C_{pv} \dfrac{dT_{pv}}{dt} = A_{mod}[\tau_g \alpha_{pv} G\beta + h_c^{g-pv}(T_g - T_{pv}) - h_c^{pv-t}(T_{pv} - T_t)], \\ \quad - \mathscr{P}_{el} \\ M_t C_t \dfrac{dT_t}{dt} = A_{mod}[\tau_t \alpha_t G(1-\beta) + h_c^{pv-t}(T_{pv} - T_t) - h_v^{am}(T_t - T_{am})] \end{cases} \quad (1)$$

where the left-hand side in the expressions denotes the variation in internal energy within each component. The right-hand side signifies the disparity between energies received and lost by the component through radiative, convective, and conductive heat exchanges. The heat exchanges use heat transfer coefficients: $h_r$ for radiative, $h_v$ for convective, and $h_c$ for conductive heat transfer. Here, $M$ [kg] denotes the mass, $C$ [J kg$^{-1}$ K$^{-1}$] represents the specific heat capacity, $T$ [K] stands for temperature, and $dt$ [s] represents the chosen time step. The above model of the PV module mainly refer to Ref. [32]. The electric power $\mathscr{P}_{el}$ generated by the PV component of the module can be expressed as follows:

$$\mathscr{P}_{el} = \mathscr{P}_s \eta_{el}, \quad (2)$$

where the available solar energy on the tilted surface, is calculated by,

$$\mathscr{P}_s = G A_{mod}, \quad (3)$$

where $G$ is the solar radiation and $A_{mod}$ is the module area ($L^*W$). The electrical performance of PV and PVT collector as a function of temperature, is given by

$$\eta_{el} = \eta_{el,ref}\left[1 + \beta_p(T_{pv} - T_{pv,ref}) + \delta ln\frac{G}{G_{ref}}\right], \quad (4)$$

where the PV module utilizes crystalline silicon (c-Si) PV cells, with a reference electrical efficiency of approximately 20% at the standard testing conditions ($G_{ref}$: 1000 W m$^{-2}$, $T_{pv,ref}$: 25 °C and $V_w$: 0 m s$^{-1}$). The temperature coefficient ($\beta_p$) is −0.25%/K and solar radiation coefficient ($\delta$) is 0.052. It is important to emphasize that the temperature coefficient can fluctuate within the range of −0.15 to −0.45%/K, depending on the specific cell technology employed. In previous research (for PVT collectors), the reference PV module efficiency taken into consideration was around 12%–15% [33–35]. However, given the efficiency trend for c-Si modules in mass production, which can now attain between 21%–23% module efficiency [36], a higher number has been chosen in this work.

### 2.2. Solar thermal module

Fig. 1(b) shows a diagram of the glazed ST collector. The flow dynamics is illustrated in Fig. 1(d), illustrating how heat is exchanged between the components: a glass cover, confined air space, the absorber plate, a metallic tube with a bond, a water channel, and a thermally insulated frame. An air gap is integrated to mitigate heat losses resulting from convection and radiation. To simplify the thermal model, following assumptions have been made:

- Neglecting heat transfer between the ground and panel.
- Pressure losses are neglected.
- The temperature is uniform across each layer and the mass flow rates in all the tubes is identical.
- Thermo-physical properties of different materials are independent of temperature.
- The radiation heat exchange at the bottom and edge losses are neglected due to the minimal temperature difference at the bottom.
- Water is utilized as heat extraction medium however, other fluids such as pure glycol or water mixed with glycol can be used.

The mentioned assumptions are indeed part of the model's simplifications, it is essential to emphasize that these assumptions are considered minor in the context of the overall model [31]. The governing dynamic energy balance equations for each component of the water-based ST collector (i.e. glass, air-gap, absorber, metallic tube, fluid circulating and an insulator) can be expressed as:

$$\begin{cases} M_g C_g \dfrac{dT_g}{dt} = A_{mod}[\alpha_g G + h_r^{g-s}(T_s - T_g) + h_v^{am}(T_{am} - T_g) \\ \quad - h_v^{g-cf}(T_g - T_{cf}) + h_r^{g-ab}(T_{ab} - T_g)] \\ M_{cf} C_{cf} \dfrac{dT_{cf}}{dt} = A_{mod}[h_v^{cf-ab}(T_{ab} - T_{cf}) - h_v^{cf-g}(T_{cf} - T_g)] \\ M_{ab} C_{ab} \dfrac{dT_{ab}}{dt} = A_{mod}[\tau_g \alpha_{ab} G - h_r^{g-ab}(T_{ab} - T_g) - h_v^{ab-cf}(T_{ab} - T_{cf})] \\ \quad - A_{ab-m} h_c^{ab-m}(T_{ab} - T_m) - A_{ab-i} h_c^{ab-i}(T_{ab} - T_i) \\ M_m C_m \dfrac{dT_m}{dt} = A_{ab-m} h_c^{ab-m}(T_{ab} - T_m) - A_{mi} h_c^{m-i}(T_m - T_i) \\ \quad - A_{mw} h_v^{m-w}(T_m - T_w) \\ M_w C_w \dfrac{dT_w}{dt} = A_{mw} h_v^{m-w}(T_m - T_w) + \dot{m}_w C_w (T_{w,i} - T_{w,o}) \\ M_i C_i \dfrac{dT_i}{dt} = A_{mi} h_c^{m-i}(T_m - T_i) + A_{ab-i} h_c^{ab-i}(T_{ab} - T_i) \\ \quad - A_{mod} h_v^{i-am}(T_i - T_{am}) \end{cases} \quad (5)$$

Descriptions regarding the evaluation of the aforementioned heat transfer coefficients can be found in [21,32,37,38]. Here, $T_{w,i}$ represents the inlet temperature of the channel, while $T_{w,o}$ indicates the outlet temperature of the water channel. The mean temperature ($T_w$) is calculated as:

$$T_w = \frac{T_{w,i} + T_{w,o}}{2} \quad (6)$$

Thermal efficiency is described as the ratio of the useful energy gain or instantaneous thermal power to the incident solar energy within a given time period and the most common expression is;

$$\eta_{th} = \frac{\mathscr{P}_{th}}{\mathscr{P}_s} = \frac{\dot{m}_w C_w (T_{w,o} - T_{w,i})}{\mathscr{P}_s}. \quad (7)$$

### 2.3. Water-based PVT collector

Water-based PVT combines elements from both PV and ST modules. This design feature facilitates the retention of collected heat from the thermal component, thereby enabling the system to yield more usable energy for heating applications. Fig. 1(c) depicts the configuration of an unglazed PVT collector, which encompasses various layers: a PV module, an absorber plate, a metallic tube with a bond, a water channel, and a thermal insulator. The heat transfer equations for components of the water-based PVT collector (i.e. tedlar, absorber and metallic tube) can be expressed as follows:

$$\begin{cases} M_t C_t \dfrac{dT_t}{dt} = A_{mod}[\tau_t \alpha_t G(1-\beta) + h_c^{pv-t}(T_{pv} - T_t)] - A_{t-m} h_c^{t-m}(T_t - T_m) \\ \quad - A_{t-ab} h_c^{t-ab}(T_t - T_{ab}) \\ M_{ab} C_{ab} \dfrac{dT_{ab}}{dt} = A_{t-ab} h_c^{t-ab}(T_t - T_{ab}) - A_{ab-m} h_c^{ab-m}(T_{ab} - T_m) \\ \quad - A_{ab-i} h_c^{ab-i}(T_{ab} - T_i) \\ M_m C_m \dfrac{dT_m}{dt} = A_{tm} h_c^{t-m}(T_t - T_m) + A_{ab-m} h_c^{ab-m}(T_{ab} - T_m) \\ \quad - A_{mi} h_c^{m-i}(T_m - T_i) - A_{mw} h_v^{m-w}(T_m - T_w) \end{cases} \quad (8)$$

The assumptions and heat transfer coefficients used for the flat plate thermal collector in Section 2.2 are similarly applied to the PVT model. Notably, this collector is unglazed, and a protective glass cover is added directly above the PV cell layer without an air gap. Additionally, the energy balance equations for the glass and PV cell components in this model are the same as those outlined in Section 2.1. Similarly, the energy balance equations for the working fluid and insulator components align with those in Section 2.2.

To solve the system of ordinary differential equations (ODEs) representing the energy conservation for each component of a collector, MATLAB's ode23 solver is used. This solver iteratively computes the solution by advancing the numerical approximation in small time steps. By providing initial conditions and the energy balance equations for each component, ode23 calculates the temperature profiles, allowing the evaluation of both the electrical and thermal performance of the collectors over time. When solving ODEs numerically, smaller time steps generally lead to more accurate results. However, larger time steps can significantly speed up the computation, though this may come at the cost of some accuracy in temperature predictions.

The exergy efficiency of the thermal module is the ratio of exergy gained by the working fluid that is useful to the solar exergy absorbed by the module.

$$\eta_{ex} = \frac{\mathscr{E}_{th}}{\mathscr{E}_{sun}}, \tag{9}$$

where the thermal exergy represents the maximum amount of work that can be extracted from the system. It measures the quality of the thermal energy, with higher temperature heat representing higher quality and consequently, higher exergy. This can be determined using the following equation [37]

$$\mathscr{E}_{th} = \dot{m}_w C_w \left[ \left(T_{w,o} - T_{w,i}\right) - T_{am} \ln\left(\frac{T_{w,o}}{T_{w,i}}\right) \right] \tag{10}$$

and the solar exergy absorbed by the PV module is calculated using the following equation [39].

$$\mathscr{E}_{sun} = \mathscr{P}_s \left(1 - \frac{4}{3}\frac{T_{am}}{T_{sun}} + \frac{1}{3}\left(\frac{T_{am}}{T_{sun}}\right)^4\right), \tag{11}$$

where $T_{sun}$ denotes the surface temperature of the sun, which is set at 5505 °C.

### 2.4. Aquifer thermal energy storage

The ATES systems provide a sustainable method for storing surplus thermal energy in underground aquifers. When combined with PVT and ST collectors, excess thermal energy generated during summer can be efficiently stored in the aquifer for later use, as illustrated in Fig. 2. By integrating the HP, renewable energy utilization is further optimized, enabling the extraction of stored energy when required for SH and DHW supply. These systems are particularly advantageous as energy storage solutions, effectively balancing seasonal energy demands. They serve as excellent mediums for storing energy, especially in the form of heat or cold. The energy is circulated between the wells, depending on the seasonal needs. For example, cold groundwater extracted during the winter can be used for cooling during summer, and vice versa, effectively using the aquifer as a seasonal thermal energy storage system. The system automatically sizes itself meaning the number of solar collectors and the size of aquifers are determined with the given energy demand and other input parameters. The integrated system can work for several different cases if the inputs are provided, making it a dynamic system working for different set of conditions.

#### 2.4.1. Aquifer model

The design of an ATES system involves calculating the optimal spacing between the two aquifers to minimize thermal interference and maximize energy recovery. This depends on the geometric shape of the thermal volume of the aquifer [41]. The hydraulic radius, representing the radius of the cylindrical volume of injected water, can be calculated using the following expression [42];

$$R_h = \sqrt{\frac{V_a}{n\pi L_a}} \tag{12}$$

where $V_a$ is the injected volume, $n$ is the porosity and $L_a$ is the screen length of the aquifer. A screen length is the section of the well installed in the aquifer to allow water exchange during thermal storage and recovery. A relation between hydraulic radius and thermal radius ($R_{th}$) was approximated using;

$$R_{th} = \sqrt{\frac{c_w V_a}{c_a \pi L_a}} \approx 0.66 R_{\mathrm{h}}, \tag{13}$$

where $c_w$ and $c_a$ are the volumetric heat capacities of water and the aquifer material. This equation [43] helps to determine the spread of thermally influenced zones around the wells. This is important for the placement of aquifers when there are more than one set of aquifers (more than one cold and one warm aquifer). This ensures that there is no thermal interaction between the aquifers.

According to Kanawala [44], the ratio of the well screen length over the thermal radius ($L_a/R_{th}$) determines the cylindrical shape of the thermal zone. A small $L_a/R_{th}$ ratio means that the thermal radius is large compared to the length of the well screen so that the cylinder is short and wide. In practice, this ratio varies roughly between 1 and 4 [41]. When infiltration continues, advective heat transport dominates. The increase in infiltration volume overtakes dispersion losses near the well, creating a sharp heat interface. This persists during infiltration as injected heat moves faster than conduction. Storage and extraction make the interface less acute due to conduction. The retained heat enhances efficiency over multiple storage cycles. To reduce losses, there is a need to minimize thermal cylinder surface area $A_a$ compared to stored heat volume $V_a$ by choosing the appropriate screen length for the required storage volume and local conditions.

$$\frac{A_a}{V_a} = \frac{2\pi R_{\mathrm{th}}^2 + 2\pi R_{\mathrm{th}} L_a}{\pi R_{\mathrm{th}}^2 L_a} = \frac{2}{L_a} + \frac{2}{R_{\mathrm{th}}}, \tag{14}$$

where the optimal screen length as a function of storage volume can be expressed as [45];

$$L_a \approx 1.02 V_a^{1/3}. \tag{15}$$

#### 2.4.2. Operational parameters of ATES system

Designing an ATES system involves optimizing various parameters to ensure efficient thermal storage and retrieval. One crucial design parameter is the volume ratio ($\eta_{vol}$). This helps in determining the effective aquifer volume used for thermal storage relative to the total volume occupied by the system and can be found using [46].

$$\eta_{vol} = \frac{V_{\mathrm{storage}}}{V_{\mathrm{occupied}}}, \tag{16}$$

where $V_{\mathrm{storage}}$ represents the aquifer volume effectively used for storage and $V_{\mathrm{occupied}}$ is the total volume occupied by the system. Another key aspect of this system is the energy ratio ($\eta_E$), defined as the annual energy extracted divided by the maximum energy stored in the occupied aquifer volume, given by [46].

$$\eta_E = \frac{E_{\mathrm{extracted}}}{V_{\mathrm{occupied}} \Delta T C_{aq}}, \tag{17}$$

where $E_{\mathrm{extracted}}$ is the annual energy extracted, $\Delta T$ is the temperature difference between the injection and extraction that is approximately 10 °C and $C_{aq}$ is the specific heat capacity of the aquifer material. The energy ratio of the modeled ATES system is not defined since there are many components involved and that makes it difficult to quantify the aquifer's performance for a give time period.

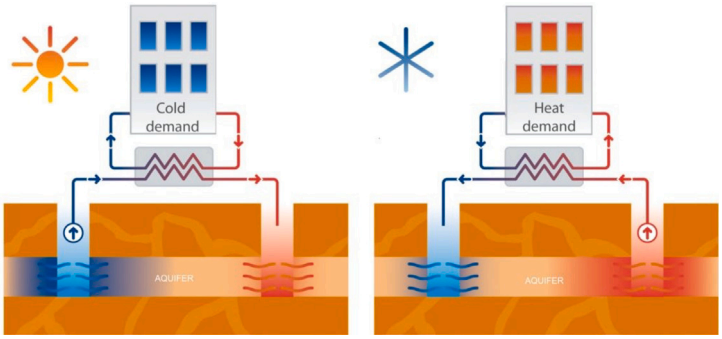


**Fig. 2.** Basic working principle of an ATES system.
*Source:* Reproduced from Huntkey [40].

The design process also involves considerations of aquifer properties such as permeability, porosity, thermal conductivity, specific heat capacity, and aquifer heterogeneity. These properties affect the thermal conductivity and storage capacity. Seasonal variations in operation must be managed to balance the thermal load and maintain consistent efficiency. These operational adjustments ensure that the system remains within optimal performance parameters throughout different seasonal demands. Considering such design and operational parameters, these systems can provide a sustainable and efficient solution for thermal energy storage.

### 2.4.3. Aquifer characteristics

The sizing of aquifers is crucial for the efficient functioning of the system. Key characteristics of an aquifer that are utilized in the current model include hydraulic conductivity, porosity, and thickness as provided in Table 1. According to Kanawala [44], hydraulic conductivity determines the rate at which groundwater can be pumped and injected, significantly impacting the system's efficiency. High porosity is desirable as it allows for greater water storage capacity, while a thicker aquifer can store more water, enhancing the system's overall capacity. These factors collectively influence the volume of thermal energy that can be stored and retrieved, thus determining the system's performance. The influence of temperature on water properties is considered negligible in this model, as the variation is less than 1% of the actual value, which does not significantly impact the system. Comparative simulations using temperature-dependent values for water's specific heat capacity and density demonstrated that the system's performance remained unaffected. Aquifer temperatures remained unchanged to two decimal places. Consequently, static values for water's specific heat capacity and density are employed throughout the model. This is in line with the findings of [47,48].

### 2.4.4. ATES modeling

The ATES along with solar collectors, heat pump, heat exchanger acts as a complete system to generate, distribute and store the thermal energy. The integrated system is modeled to optimize the performance of each component, resulting in optimized performance of the overall system. To accomplish that, the system is modeled for a year (8760 h) during which the system switches between five modes. The switching conditions for each mode is carefully chosen to account for changes throughout the year for several parameters such as irradiance, demands and aquifer temperature. The system in general is a closed loop meaning there is no loss of water at the end of cycle (here, it is one year).

## 2.5. Heat pump

A heat pump operates on the principle of moving heat rather than generating it, making an environmental friendly choice for heating and cooling needs. It can extract heat from the air, ground, or water sources,

**Table 1**
Hydraulic and thermal properties of the aquifer and clay layer, [49].

| Symbol | Value |
|---|---|
| $n$ | 0.30 |
| $k_{h,aq}$ | 35 m $d^{-1}$ |
| $k_{v,aq}$ | 7 m $d^{-1}$ |
| $k_{h,aqt}$ | 0.05 m $d^{-1}$ |
| $k_{v,aqt}$ | 0.01 m $d^{-1}$ |
| $\rho_{sc}$ | 2640 kg $m^{-3}$ |
| $\rho_w$ | 998 kg $m^{-3}$ |
| $k_{aq}$ | 3 W $m^{-1}$ $K^{-1}$ |
| $k_{aqt}$ | 1 W $m^{-1}$ $K^{-1}$ |
| $k_w$ | 0.60 W $m^{-1}$ $K^{-1}$ |
| $C_{aq}$ | 710 J $kg^{-1}$ $K^{-1}$ |
| $C_w$ | 4186 J $kg^{-1}$ $K^{-1}$ |

depending on the type of system. Additionally, their is another type of a HP which is a hybrid source and combines two or more types of a HP. The extracted heat can then be distributed throughout a building to provide warmth during colder months or expelled to provide cooling during warmer months. When combined with ST or PVT collectors, the COP and sustainability of a HP system can be further enhanced. Thermal collectors or seasonal storage can supplement the energy input required by the HP, thereby reducing its overall energy consumption and environmental impact. The regular COP of a HP is defined as the ratio between heat generation and electricity consumption, fluctuates over time and is given by

$$COP = \frac{Q_h(t)}{E(t)} \tag{18}$$

The work required for compression in a thermodynamic process can be calculated using the following equation

$$W_{Comp} = \frac{P_1 \cdot v_1}{\eta_{comp}} \left(\frac{k}{k-1}\right) \left[\left(\frac{P_2}{P_1}\right)^{\frac{k}{k-1}} - 1\right], \tag{19}$$

where $P_1$ is the initial pressure of gas before compression and $P_2$ is final pressure after compression, $k$ is the ratio of specific heats, is approximately 1.106 for R-134a (tetrafluoroethane), $\eta_{comp}$ is the efficiency of compressor and $v_1$ is the specific volume of the gas before compression. R134a is a refrigerant widely used in HPs due to its favorable thermodynamic properties, offering high energy efficiency, low toxicity, and a non-flammable classification.

This study utilizes a thermodynamic cycle to better quantify the heat transferred for heating demand [50]. Fig. 3(a) presents the components of the HP, divided into four parts: evaporation (D to A), compression (A to B), condensation (B to C), and expansion (C to D). In parallel, the thermodynamic cycle of a HP is solved hourly, considering fluctuating thermal conditions for both SH and DHW. The cycle begins at point D, where the coolant absorbs heat in the evaporator as shown in Fig. 3(b). The coolant changes from a liquid to a gas through evaporation, rather than increasing its temperature, reaching

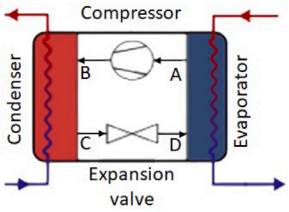


(a) Thermodynamic processes in HP.

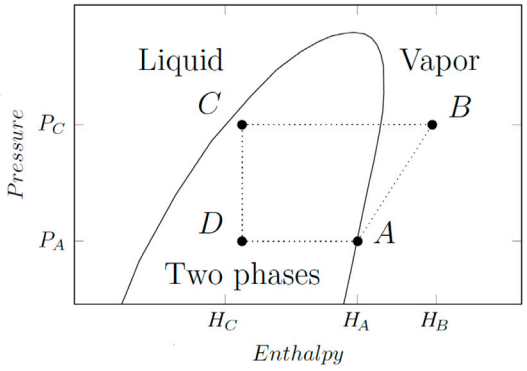


(b) A HP thermodynamic cycle represented on a *P-H* diagram.

**Fig. 3.** Simplified heat pump diagram illustrating the thermodynamic cycle.
*Source:* Adapted from Aguilera [50].

point A. Leaving the evaporator, the coolant in its gaseous phase is compressed by a compressor, increasing both pressure and temperature, reaching point B. Next, in the condenser, the coolant releases heat and condenses, reaching point C. Finally, the fluid returns to point D through pressure reduction in an expansion valve, completing the cycle. A constant evaporator temperature of 0 °C is assumed to solve the thermodynamic cycle where point A is assumed to be a saturated gas and the enthalpies at points B and C are determined using a fitted COP expression [51].

The thermodynamic cycle modeling depicted in Fig. 3(b) is to be solved for each hour of the year, taking into account the fluctuating thermal conditions used for both SH and DHW. These conditions are based on the cycle suggested by Chaturvedi et al. [52]. The COP of the HP is determined by including these thermodynamic considerations in the current statistical data model and the thermodynamic considerations of model developed by [51]. This computation is based on the sink temperature $T_{sink}$ which is then calculated, required for heating.

$$T_C = T_{sink} + T_{cond}, \tag{20}$$

The heat source temperature is determined by either the output of a thermal collector or the input from a seasonal storage, depending on the selected heating mode. Heat sink temperatures are determined for floor heating, radiator heating and DHW. For floor heating and radiators, temperature profiles are derived from the hourly interpolated ambient temperature using

$$T_{sink} = \begin{cases} 40\ °C - 1.0\ T_{am}, & for\ radiator\ heating \\ 30\ °C - 0.5\ T_{am}, & for\ floor\ heating \end{cases} \tag{21}$$

It should be noted that for DHW, an unfixed heat sink temperature is used. When the temperature is within the range of 60–65 °C, the constraint for DHW is expressed as:

$$60\ °C \leq T_{sink} \leq 65\ °C \tag{22}$$

The constraint for the warm water supply is that the supplied flow rate is equal to the required flow rate.

## 3. Integration and operational modes

The system consists of solar collectors, HP, heat exchanger, and ATES seasonal storage. These components can be integrated into one reliable, resilient system with high-performance efficiency, storage of thermal energy, and ensuring year-round availability. The thermal energy can be used to provide cooling, SH and DHW for the buildings. For instance, ST/PVT collectors can supply excess heat to an ATES during summer, enhancing the heat supply. Similarly, during winter, the stored heat can be used in conjunction with the HP to provide heating, thereby improving the COP of the HP for the integrated system. The heat exchanger plays a crucial role in transferring heat between the ATES system and the building's heating or cooling demand, ensuring efficient energy use and minimal losses. This integration not only improves energy efficiency but also contributes to a more resilient and flexible energy system. It is capable of reducing dependency on fossil fuels and decreasing greenhouse gas emissions. The strategic combination of these technologies is pivotal in advancing towards a more sustainable and energy-efficient future.

This system was designed for heating/cooling requirements of a residence, as well as to fulfill its DHW needs. In most of the cases, a HP based systems prioritize DHW production. However, in the present study, SH takes precedence over DHW. While DHW is important for daily use, SH is usually prioritized in colder months due to its higher demand and immediate need. DHW can often be stored, making it more flexible in system operation.

### 3.1. System description

A schematic view of the system is illustrated in Fig. 4 which consists of several parts, namely

- a PV module (including PV module in a PVT), generates electricity to the integrated system (power pumps, heat pump) and electrical load.
- a thermal module (including thermal module in a PVT), produces warm water for domestic use through the absorption of solar energy and subsequent heat transfer processes.
- an ATES system, utilizes the subsurface thermal energy to provide both heating and cooling for buildings through a process of seasonal thermal energy storage and extraction.
- a HP extracts heat from a low-temperature heat source, such as solar collector output or the ground aquifer, and transfers it to a higher temperature to provide SH or DHW. Additionally, in cooling mode, the HP can reverse its operation, removing heat from the indoor environment to achieve cooling.
- a heat exchanger, facilitates the transfer of thermal energy between two fluids, enabling efficient heating, cooling, or heat recovery.
- circulation pumps, to circulate the fluids within the system, ensuring a continuous flow through the collector and facilitating efficient heat transfer between the collector and the heat transfer fluid.

A few assumptions have been taken into account for the proposed system, such as:

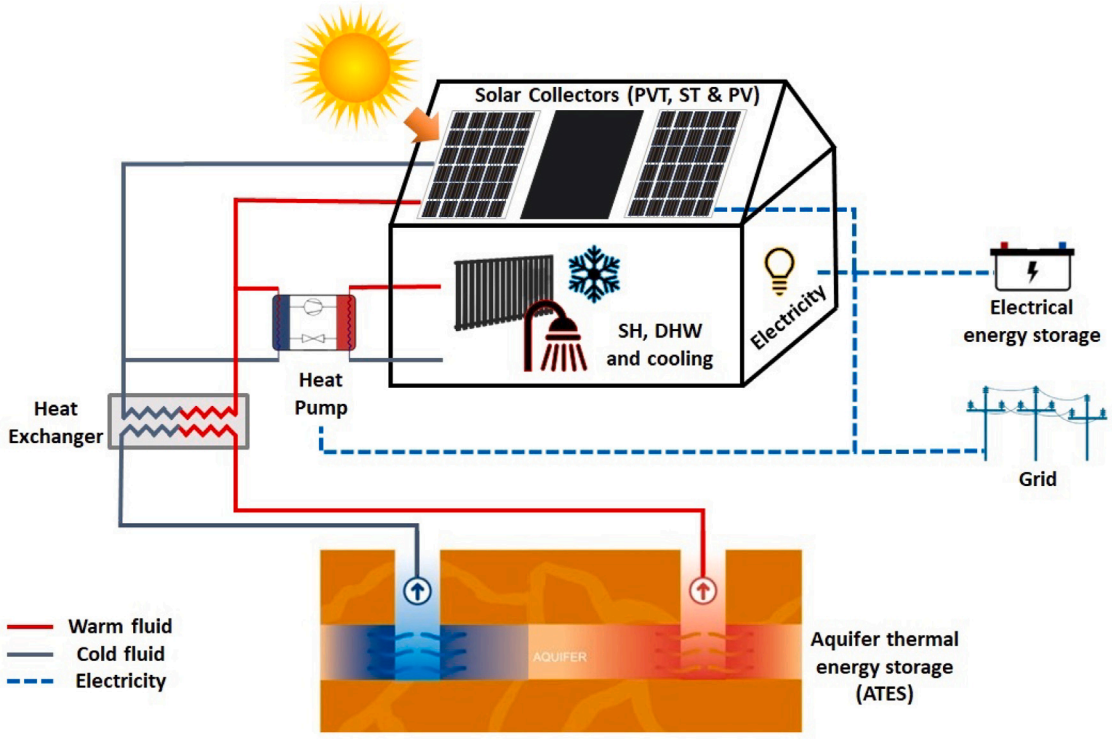


**Fig. 4.** Schematic diagram of a solar system combined with solar collectors, a heat pump, an ATES, a heat exchanger and an electrical storage.

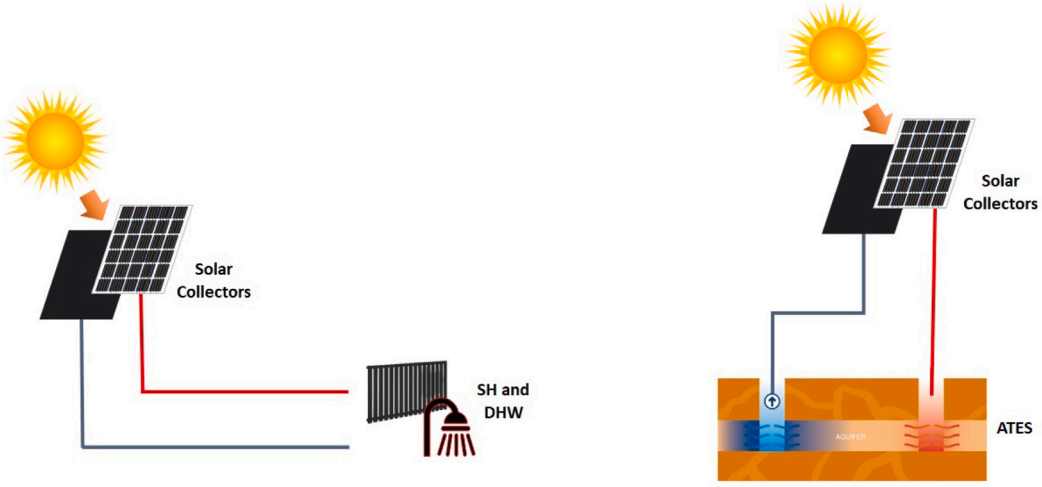


(a) Mode I (a): Solar heating mode

(b) Mode I (b): Underground storage mode

**Fig. 5.** Classification of Mode I for SH, DHW, and storage of heat generated by the collectors.

- optical characteristics of the collectors components are assumed as constant [53].
- collectors are assumed to be well-insulated, with no significant heat losses to the surroundings [38].
- losses at bends, valves, and other components are assumed to be negligible [54].
- constant fluid properties, within the operating temperature range [55].
- the flow rate of the fluid within the module remained constant across all pipes [53].
- uniform temperature and composition throughout the aquifers [28].
- the heat exchanger is assumed to operate with an effectiveness of 90%.
- pressure drops and losses across the components of system are assumed to be negligible [56].
- pipes connecting the system components are well-insulated, resulting in negligible heat loss to the surroundings [57].
- The electricity required for pumping liquids is not considered, as thermal energy output far exceeds electrical consumption. Water is pumped only during operational periods, unlike continuous systems, resulting in significantly lower overall electrical energy use, which accounts for only 1% of the total energy delivered [58].

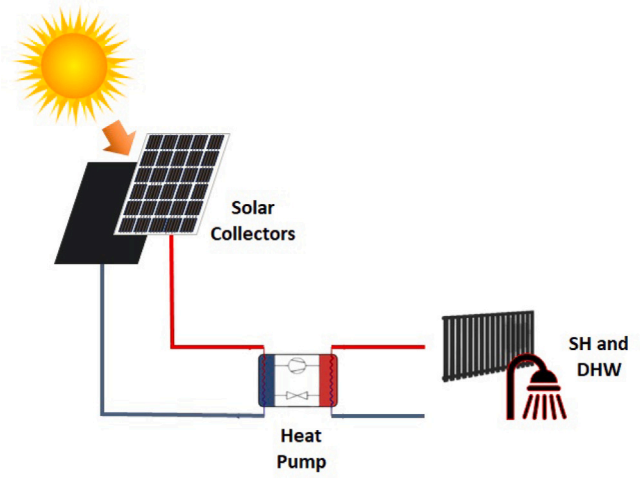


**Fig. 6.** Mode II: The HP heating mode for SH and DHW coverage.

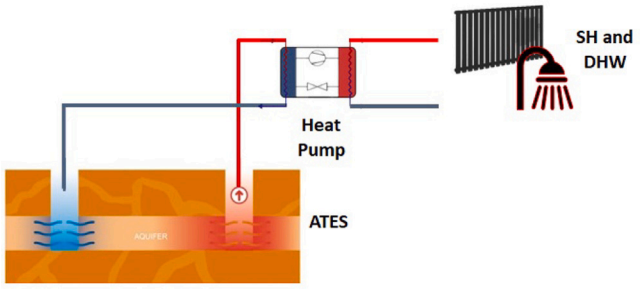


**Fig. 7.** Mode III: The HP storage mode for SH and DHW coverage.

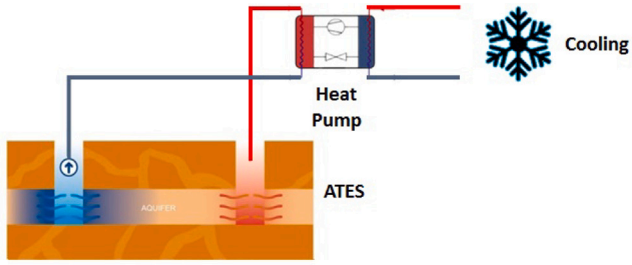


**Fig. 8.** Mode IV: Operational mode for cooling.

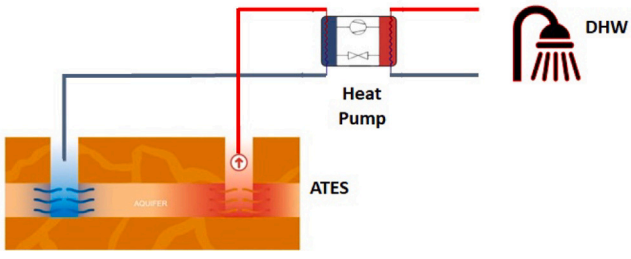


**Fig. 9.** Mode V: Heating mode for DHW coverage.

It should be noted that the mentioned assumptions are indeed part of the system simplifications, it is essential to emphasize that these assumptions are considered minor in the context of the overall system model.

### 3.2. Operational modes

The system operates in distinct modes, utilizing a series of switches to direct heat flow based on supply and demand. The classification of system configurations considering these distinct modes for SH, DHW, and cooling is presented as follows:

- Solar heating and underground storage mode (Mode I) is split into two parts as illustrated in Fig. 5. Solar heating part (see Fig. 5(a)), extract heat directly from solar collectors, typically utilized during the milder seasons of spring or autumn. This mode activates when the temperature of the heat extraction medium rises to supply heating, as demonstrated in the following equations. It accounts for the mass flow rate and temperature variations each hour throughout the year to deliver the required heating and following conditions must be met;

$$T_{w,o} > \begin{cases} 40\ ^{\circ}\mathrm{C} - 1.0\ T_{am}, & for\ radiator\ heating \\ 30\ ^{\circ}\mathrm{C} - 0.5\ T_{am}, & for\ floor\ heating \end{cases} \tag{23}$$

  and for DHW, the following condition must be met;

$$T_{w,o} > 60\ ^{\circ}\mathrm{C} \tag{24}$$

  Throughout the year, a significant portion of the heat produced by solar collectors is generated during the summer, when household heating is typically unnecessary. To prevent this surplus heat from going to waste, it is stored in underground warm aquifers using the ATES system as depicted in Fig. 5(b), providing an efficient solution for conserving the excess energy for winter use.
- The HP heating mode (Mode II) integrates solar collectors output with a HP as shown in Fig. 6 to achieve the desired heating temperature, termed as the HP heating mode. This mode activates when the conditions outlined in the above equations are not satisfied, or when the heat supplied by Mode I is insufficient. However, for this mode to operate, the given condition must be met.

$$T_{w,o} > 20\ ^{\circ}\mathrm{C} \tag{25}$$

  By employing the heat pump, a higher temperature can be reached, allowing the system to partially meet the heating demand.
- The HP storage mode (Mode III) presented in Fig. 7, involves the utilization of a HP in conjunction with ATES for heating purposes, predominantly during the winter season. It is utilized when other modes are insufficient to meet the heat demand and this mode is expected to operate throughout the heating season.
- Transitioning to the cooling mode (Mode IV), the HP extracts heat from the building while utilizing cold water from the cold aquifer for effective cooling as presented in Fig. 8. During the summer season, SH is not necessary; however, DHW is still required. This need is met simultaneously with DHW mode, which activates when there is a demand for space cooling and cold aquifer provides the desired temperature.
- Fig. 9 presents the DHW heating mode (Mode V) where ATES, and a HP are combined to provide DHW which is required throughout the year. Since for DHW, a temperature of 60 to 65 °C is required, and solar collectors alone (i.e., Mode I) cannot achieve this temperature considering the Dutch climate, an ATES system is utilized with a HP. It is important to note that using solar collectors with a HP is another option to meet this demand during the summer; in this case, the heat is transferred to the HP instead of being stored in the warm aquifer. The preference for the HP with ATES arises from the fact that DHW is primarily needed in the morning or late evening, times when solar radiation is very limited.

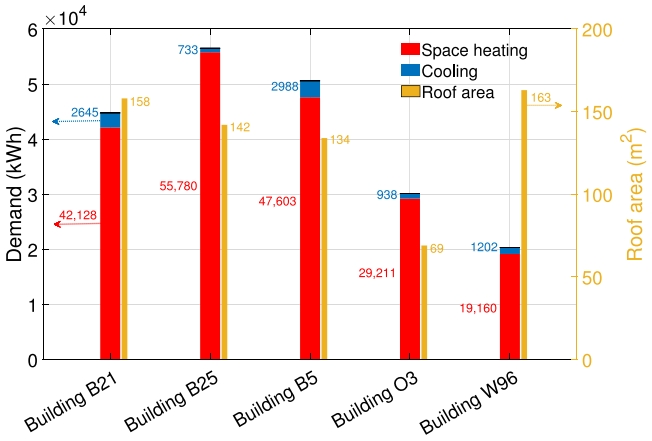


**Fig. 10.** Annual SH and cooling demand with roof area for buildings B5, B21, B25, O3 and W96 with current insulation.

The collectors operate in an islanding mode, where it continues to provide electrical power and heating/cooling independently of the grid. For optimal operation, these modes are typically managed by an intelligent control system that monitors climate data and building energy demands. This ensures that the system operates in the most efficient mode possible, balancing between electricity production, heating, and cooling needs, and energy storage. In summary, the system can operate in various modes to maximize energy efficiency and meet the dynamic energy demands of a building. Properly managed, such systems can significantly reduce energy costs and environmental impact while providing reliable and sustainable energy solutions. Specific components of the system can be isolated for maintenance without disrupting the operation of entire system. For example, maintenance on the heat pump can occur while solar collectors continue generating both heat and electricity.

## 4. Input parameters

The performance of the integrated system is significantly influenced by various parameters, including weather conditions, heating/cooling demand, solar collector type, heating system configuration, insulation type and the materials used. The aim is to assess and compare the annual and weekly performance of various configurations, focusing on identifying the most effective solution for meeting energy demands for the considered buildings in the Amsterdam region. Particular emphasis is placed on systems without natural gas to minimize electricity consumption. Initially, an analysis of the input parameters such as heating and cooling demands of the buildings, along with relevant weather data is presented.

### 4.1. Demand side inputs

The five buildings under consideration are located on three different streets in the center of Amsterdam, randomly selected from a dataset of residential buildings. They represent some of the most common roof area configurations found in the city. Due to strict Dutch privacy laws, the addresses of these buildings remain confidential. Building B5, built in 1750, has a roof area of 134 $m^2$, while building B21, constructed around the same time, has a roof area of 158 $m^2$. Building B25, dating back to 1700, features a 142 $m^2$ roof area. Building O3, built in 1685, has a smaller roof area of 69 $m^2$, whereas building W96, constructed in 1693, has the largest roof area at 163 $m^2$. Building W96 has three floors, building B21 has five, and the other three buildings have four floors each. The annual SH and cooling demands for these buildings, based on their current insulation levels and influenced by dynamic occupant behavior, are shown in Fig. 10. In contrast, Fig. 11 depicts the hourly variation for all five buildings, reflecting the seasonal fluctuations in their energy needs.

For all the five buildings, three levels of insulation have been established based on recognized standards: 1) current, 2) medium temperature ($T_M$) and 3) low temperature ($T_L$). Considering SH and cooling demand for all the five buildings, shown in Fig. 12:

- The current level is considered as the base scenario, e.g. the worst-case scenario [59]. It represents the energy demand in its original state with an annual total SH demand of approximately 194 MWh.
- If renovated to the $T_M$-level, where SH demand is less than 80 kWh $m^{-2}$ yearly and the supply temperature required is 70 °C, the annual total SH demand decreases to almost half, around 95 MWh.
- However, the $T_L$-level renovation provides the most significant improvement, achieving near-ideal insulation with a SH demand of less than 50 kWh $m^{-2}$ per year and a supply temperature of 55 °C. As a result, the total SH demand is minimized to just 50 MWh, representing the lowest possible level.

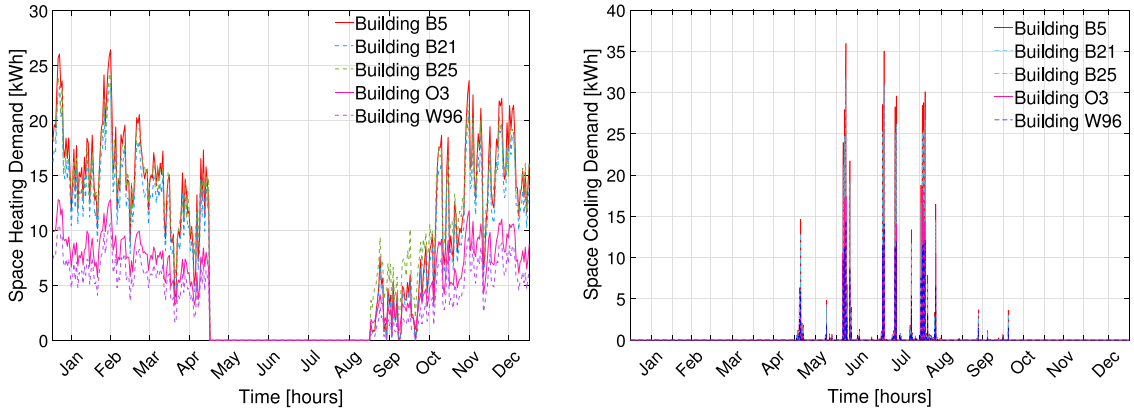


(a) SH demand (b) Cooling demand

**Fig. 11.** Hourly variation of SH and cooling demand for buildings B5, B21, B25, O3 and W96 with current insulation.

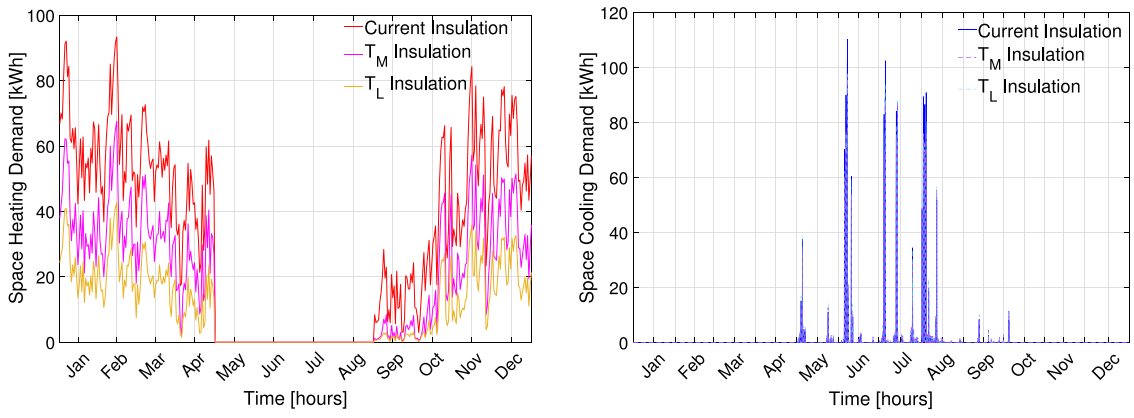


(a) SH demand (b) Cooling demand

**Fig. 12.** Total SH and cooling demand for all the considered buildings with different insulation levels.

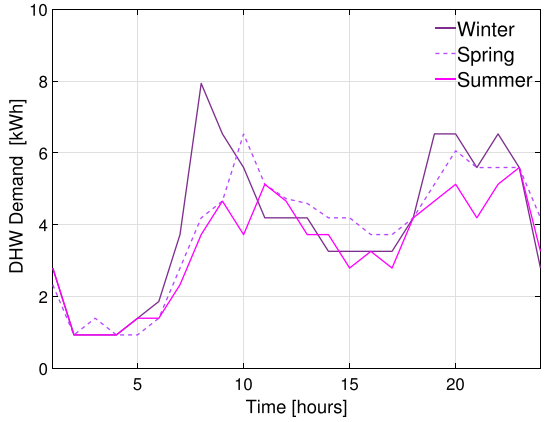


**Fig. 13.** Daily DHW demand for building B5 considering multiple seasons.

The $T_M$ and $T_L$-levels are defined by the Municipality of Amsterdam. They indicate that buildings with a yearly heat demand below 80 kWh m$^{-2}$ of floor area can be heated with a system delivering heat at middle temperature. Additionally, a maximum heat demand of 50 kWh m$^{-2}$ is stated for $T_L$ heat strategies [60]. The supply temperature used in this research is based on the supply temperature for low-temperature heating, as described by van Egmond and van Petersen [61]. The load data is based on dynamic simulations conducted in Ladybugtools using OpenStudio and EnergyPlus. The models were calibrated based on benchmark values.

This progression illustrates how enhanced insulation can drastically reduce heating demand, promoting greater efficiency and sustainability. Considering these buildings, the total cooling demand is 8506 kWh with current insulation, decreases to 8411 kWh with $T_M$-level insulation and increases to 8604 kWh with $T_L$-level insulation. This shows that improved insulation primarily benefits heating efficiency, while cooling demand remains relatively stable. Similarly, the DHW demand remains consistent across different insulation levels but varies noticeably with the seasons, reflecting the influence of occupant behavior and usage patterns. The annual total DHW demand for all the considered buildings remains fairly consistent throughout the year, with a slight reduction during the summer months. Fig. 13 illustrates a daily DHW profile for building B5, revealing higher demands in winter, a slight decrease in spring, and even lower requirements in summer. The DHW is required throughout the year and overall, the DHW demand exhibits minimal variation throughout the year and is approximately 92.70 MWh considering various insulation levels. By incorporating variations in occupant behavior, the study achieves a more realistic representation of energy demand, enabling a more accurate evaluation of system performance under typical residential conditions.

### 4.2. Weather data

In Fig. 14, input weather data extracted from METEONORM version 7.3 [62] is presented weekly considering distinct seasons and annually. The hourly variation of ambient temperature over a two-week period for three different seasons is presented in Fig. 14(a). For the winter weeks, ambient temperatures can drop below 0 °C, with the maximum solar radiation reaching just over 500 W m$^{-2}$. During the spring weeks, the average ambient temperature is approximately 12 °C, while solar radiation fluctuates and can peak at 900 W m$^{-2}$. For the summer weeks, the average ambient temperature rises to around 20 °C, with ample solar radiation available throughout the period. Fig. 14(b) illustrates the annual profiles of solar radiation and average ambient temperature. In all cases, similar weather conditions, including wind speed, were applied for consistency across the data.

## 5. Results and discussion

Initially, a simple comparison of only solar collectors is presented. Subsequently, various combinations were examined by considering various key factors: the type of solar collectors used, which constitutes the primary focus, the type of heating method and the level of insulation (i.e. current and new).

### 5.1. Comparison of only solar collectors performance

The performance of the solar collectors is influenced by several factors, including ambient temperature, solar irradiance, wind speed, mass flow rate, and the type of working fluid. However, the materials and thicknesses of the components, as outlined in Table 2, also play a significant role in determining efficiency. Simulations were performed using the weather data presented in Section 4 for the developed solar collector models presented in Sections 2.1, 2.2, and 2.3. These simulations assess the hourly performance of the collectors in detail. Monthly outputs of the collectors were then calculated, ultimately aiming to determine the total annual yields.

In order to compare only solar collectors performance, the fluid inflow temperature was assumed to be close to the ambient temperature, as no heat storage tank was considered for this comparison. As the data is collected, a comparison of the different efficiencies obtained from the glazed ST collector and the unglazed PVT collector is presented in Fig. 15. This figure illustrates the thermal and electrical performance

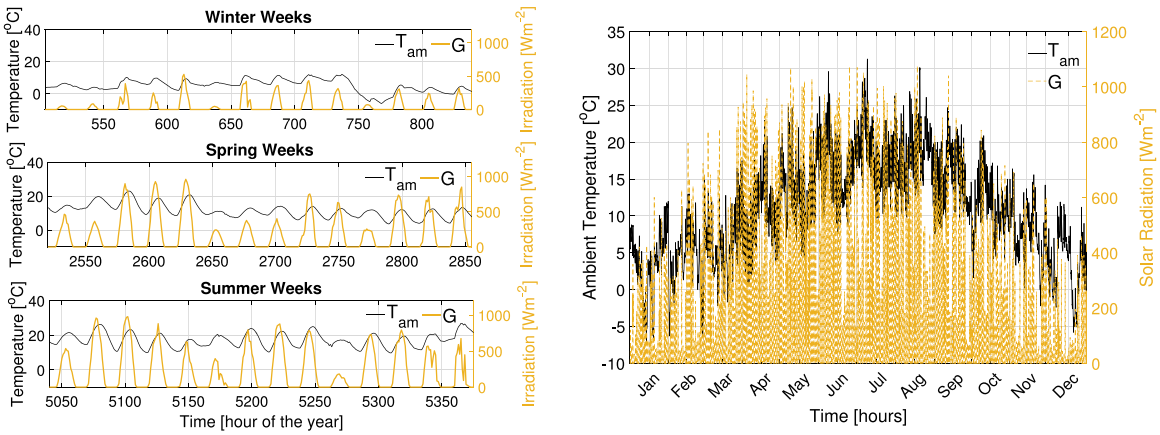


(a) Weekly (b) Annually

**Fig. 14.** Evolution of solar radiation and average ambient temperature in Amsterdam region.

**Table 2**
The used thermo-physical properties of the studied collectors [31].

| | Symbol | Value |
|---|---|---|
| Glass cover | $\alpha_g$ | 0.10 |
| | $C_g$ | 670 J kg$^{-1}$ K$^{-1}$ |
| | $\lambda_g$ | 1.10 W m$^{-1}$ K$^{-1}$ |
| | $\rho_g$ | 2200 kg m$^{-3}$ |
| | $\varepsilon_g$ | 0.88 |
| | $\ell'_g$ | 0.0032 m |
| | $\tau_g$ | 0.84 |
| PV cell | $\alpha_{pv}$ | 0.90 |
| | $\beta_p$ | −0.25%/K |
| | $C_{pv}$ | 900 J kg$^{-1}$ K$^{-1}$ |
| | $\delta$ | 0.052 |
| | $\lambda_{pv}$ | 148 W m$^{-1}$ K$^{-1}$ |
| | $\rho_{pv}$ | 2330 kg m$^{-3}$ |
| | $\eta_{el,ref}$ | 20% |
| | $\ell'_{pv}$ | 0.0003 m |
| Tedlar | $\alpha_t$ | 0.80 |
| | $C_t$ | 1200 J kg$^{-1}$ K$^{-1}$ |
| | $\lambda_t$ | 0.20 W m$^{-1}$ K$^{-1}$ |
| | $\rho_t$ | 1200 kg m$^{-3}$ |
| | $\ell'_t$ | 0.00075 m |
| Air | $C_{cf}$ | 1007 J kg$^{-1}$ K$^{-1}$ |
| | $\lambda_{cf}$ | 0.026 W m$^{-1}$ K$^{-1}$ |
| | $\rho_{cf}$ | 1.184 kg m$^{-3}$ |
| | $\ell'_{cf}$ | 0.020 m |
| Absorber and metallic tube | $\alpha_{ab/m}$ | 0.95 |
| | $C_{ab/m}$ | 385 J kg$^{-1}$ K$^{-1}$ |
| | $\lambda_{ab/m}$ | 400 W m$^{-1}$ K$^{-1}$ |
| | $\rho_{ab/m}$ | 8900 kg m$^{-3}$ |
| | $\ell'_p$ | 0.001 m |
| Water | $C_w$ | 4186 J kg$^{-1}$ K$^{-1}$ |
| | $\lambda_w$ | 0.60 W m$^{-1}$ K$^{-1}$ |
| | $\rho_w$ | 998 kg m$^{-3}$ |
| Insulation | $C_i$ | 670 J kg$^{-1}$ K$^{-1}$ |
| | $\lambda_i$ | 0.034 W m$^{-1}$ K$^{-1}$ |
| | $\rho_i$ | 20 kg m$^{-3}$ |
| | $\ell'_i$ | 0.05 m |

characteristics as a function of the operating conditions, expressed by the reduced temperature $(T_{w,i}-T_{am})/G$. It is obvious that for the glazed ST configuration, the slope of the thermal efficiency curve is higher in comparison to the unglazed PVT configuration. The efficiency curve for unglazed type configuration exhibits a more rapid reduction when contrasted with glazed type configuration. The reduced temperature also impacts the PV efficiency since the cell temperature also relies on the operating conditions that are water inlet temperature, ambient temperature, and solar radiation level. However the change in PV performance is small.

The electrical efficiency of a PV module is significantly influenced by the temperature of PV cells, which in turn is affected by various factors such as wind speed, solar radiation, and ambient temperature. PV efficiency and cell temperature are plotted against solar radiation in Fig. 16. It reveals that in the case of an unglazed PVT collector, the integration of a thermal module extracts heat from the top, thereby reducing cell temperature and enhancing electrical efficiency. Conversely, for PV only module, with the increase in solar radiation raises cell temperature, leading to lower PV module efficiency. Moreover, an increase in wind speed lowers cell temperature due to the higher convection heat transfer coefficient, which increases with greater wind speed. As mentioned earlier, hourly simulations were carried out to assess the performance of the collectors in detail with the final aim of obtaining total annual yield. Among the two configurations, the PV module in the PVT collector produces the higher electrical output, approximately 225 kWh m$^{-2}$ annually. In contrast, the standalone PV module generates the lower electrical output, around 209 kWh m$^{-2}$. This demonstrates a 7.70% gain in electrical output achieved by the PVT collector configuration. The total annual available solar irradiation for the tilted surface is 1190 kWh m$^{-2}$.

### 5.2. Weekly and annual simulations of the integrated system

The integrated system, as depicted in Fig. 4, operates in distinct modes outlined in Section 3.2, utilizing the input parameters and weather data detailed in Section 4.1. Two cases are analyzed: A) PVT collectors and B) PV/ST collectors, with each case further divided into subsections based on the type of heating and insulation.

#### 5.2.1. Case a: PVT collectors

Since each building has a different level of insulation and insulation plays a crucial role in determining energy demand, especially for SH as mentioned earlier. The results are subdivided into two parts by considering current insulation level and new insulation level. The evaluation considers both $T_M$ and $T_L$ scenarios for new insulation, as well as the type of heating system, whether radiator or floor heating is utilized.

- **Current insulation with radiator heating**
  First, current insulation scenario is utilized, with radiators used for SH. Fig. 17(a) shows the inflow and outflow temperatures of the PVT collector, with the data split into various seasons. The fluid entering the collectors matches the temperature of the cold aquifer, with losses between the aquifer and collector being

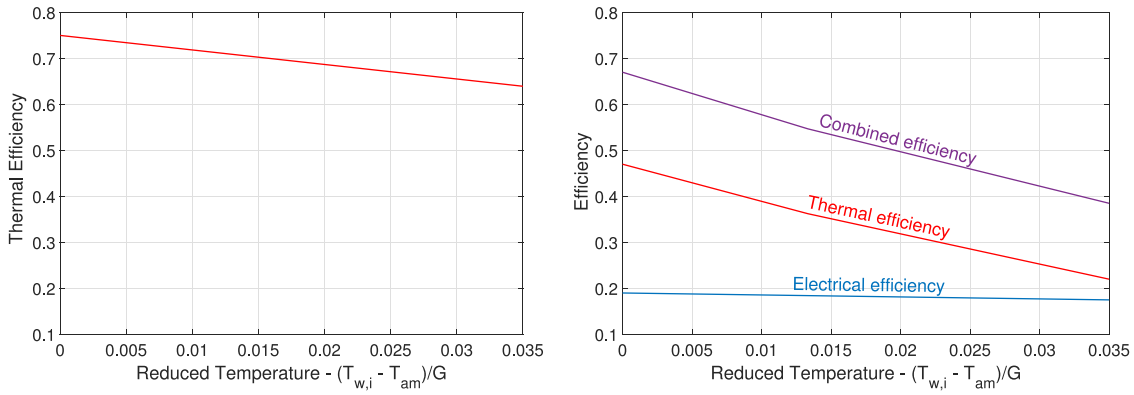


(a) Glazed ST collector (b) Unglazed PVT collector

**Fig. 15.** Simulated performance of ST and PVT including PV efficiency (blue), thermal efficiency (red), and combined efficiency (purple) as a function of operation condition. (For interpretation of the references to color in this figure legend, the reader is referred to the web version of this article.)

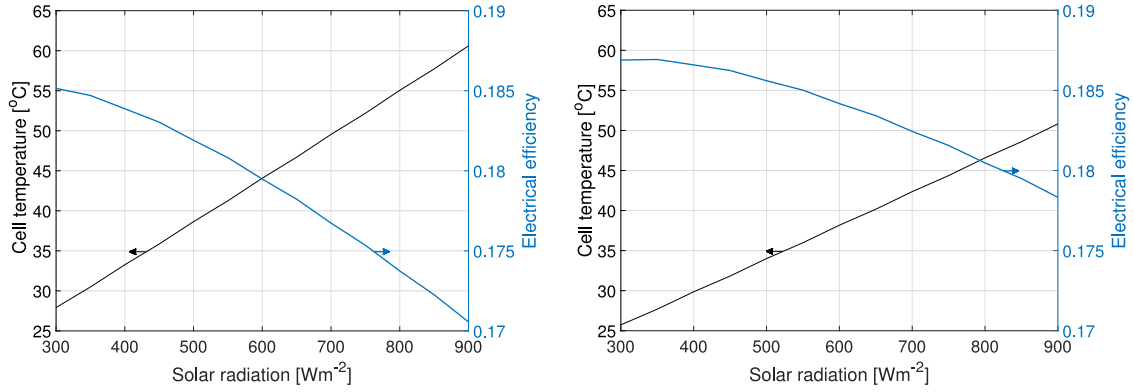


(a) Glazed PV module (b) Unglazed PVT collector

**Fig. 16.** Influence of solar radiation on the cell temperature and electrical efficiency of the unglazed PV and PVT collector.

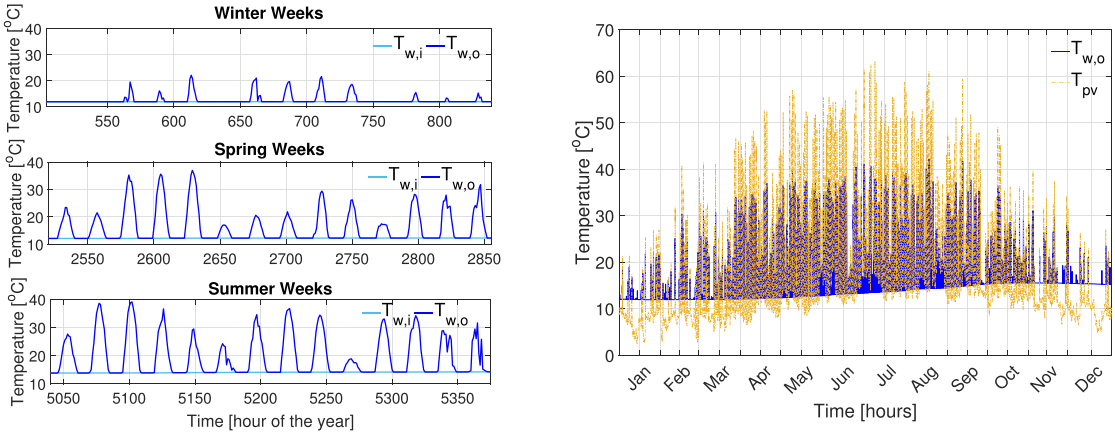


(a) Weekly variation of temperatures (b) Annual variation of outflow and PV temperatures

**Fig. 17.** Variation of inflow and outflow temperatures considering PVT collectors, current insulation and radiator heating.

negligible. During the winter weeks, the PVT outlet water temperature typically remains below 20 °C, whereas during the spring weeks, it can exceed 30 °C. The summer weeks exhibit higher outlet water temperatures, reaching up to 40 °C. In parallel, Fig. 17(b) illustrates annual outflow and PV cell temperatures. High ambient temperatures and solar radiation during the summer months increase the PV cell temperature to 60 °C, thereby reducing electrical performance.

The HP is another important component of the integrated system. The HP outlet temperatures, based on inputs from either the PVT

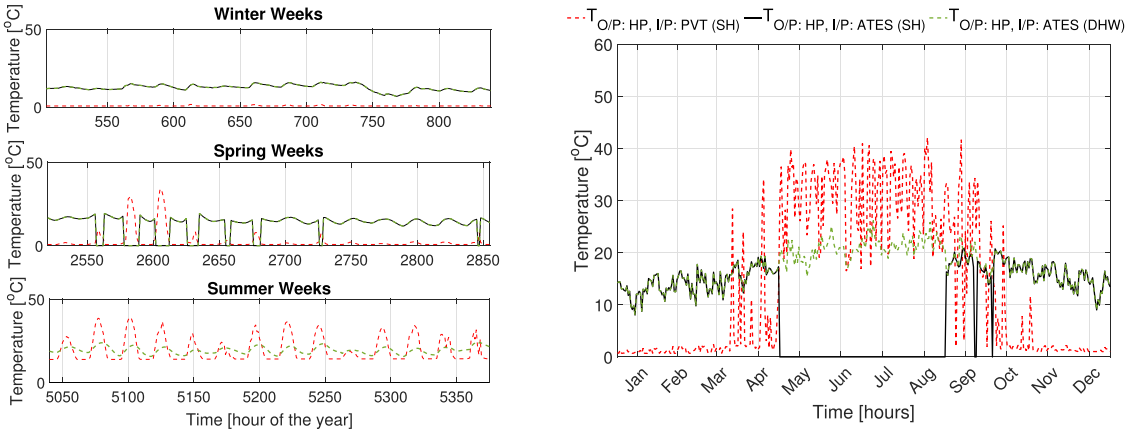


(a) Weekly variation of temperatures (b) Annual variation of temperatures

**Fig. 18.** Variation of the HP outlet temperatures (O/P) and input temperatures (I/P) to the PVT and ATES components considering PVT collectors, current insulation and radiator heating for (a) weekly and (b) annual variation of temperatures. (For interpretation of the references to color in this figure legend, the reader is referred to the web version of this article.)

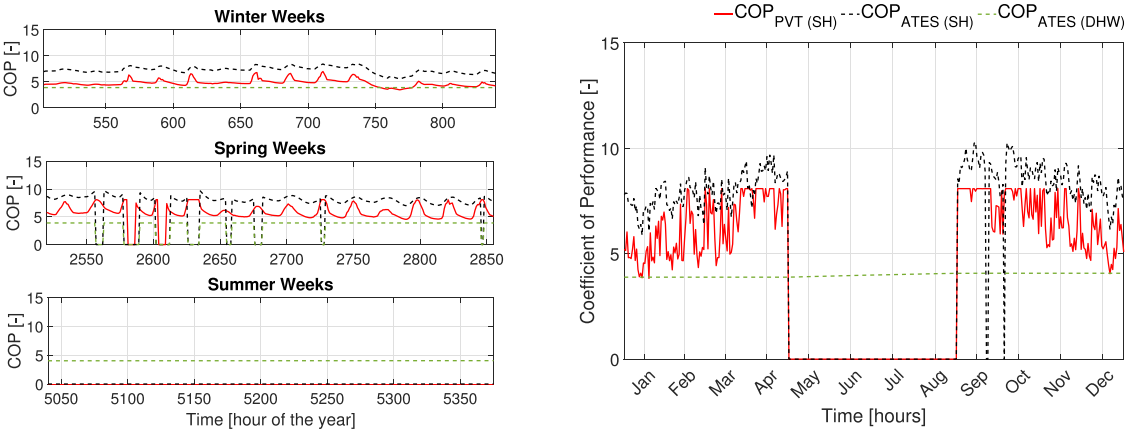


(a) Weekly variation of COP (b) Annual variation of COP

**Fig. 19.** COP of the HP with radiator heating for DHW and SH, utilizing ATES, current insulation and PVT systems for (a) weekly and (b) annual variation.

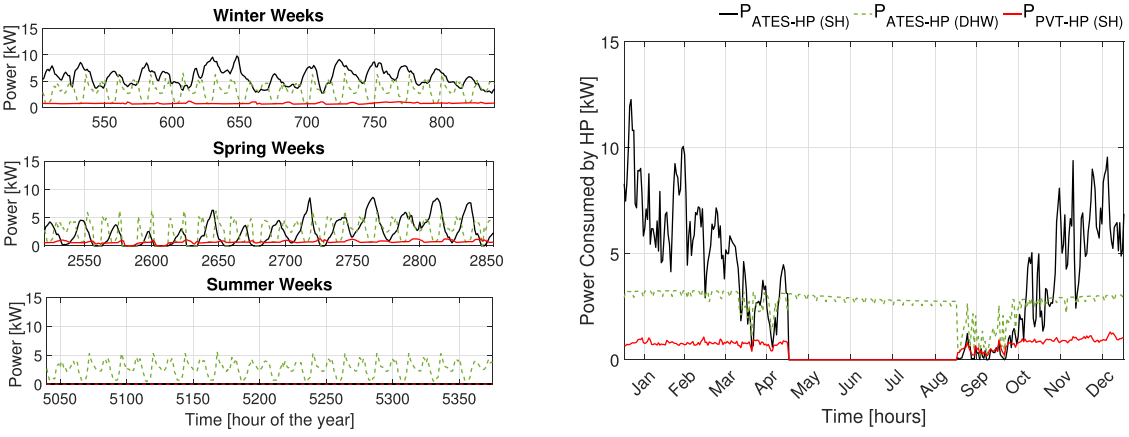


(a) Weekly variation of power (b) Average annual variation of power

**Fig. 20.** Power consumption of the HP with radiator heating for DHW and SH, utilizing ATES, current insulation and PVT systems for (a) weekly and (b) average annual variation.

collector or the warm aquifer, are shown in Fig. 18. It can be observed in Fig. 18(b) that when the PVT outlet temperature exceeds 20 °C, it is combined with the HP, and the resulting outlet temperature is plotted in red. The HP also operates with ATES, where the warm aquifer is used for SH during winter and for DHW during summer. The PVT outlet temperature is not utilized by the HP during the summer, as heat is stored in the warm aquifer, resulting in higher temperatures from the HP outlet. However, in

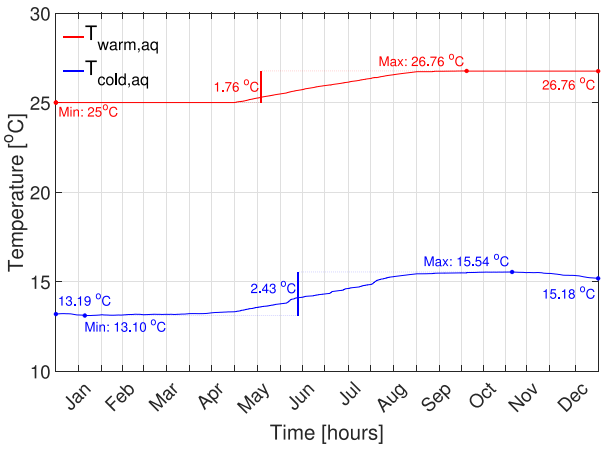


**Fig. 21.** Annual temperature variation with current insulation of the aquifers considering PVT collectors and radiator heating, highlighting their seasonal fluctuations. (For interpretation of the references to color in this figure legend, the reader is referred to the web version of this article.)

the winter, the PVT outlet is utilized by the HP, resulting in lower HP outlet temperatures. The black line represents the HP outlet temperature when combined with ATES for SH, showing that the warm aquifer, with a temperature around 25 °C, is used as input to the HP. The HP outlet temperature is slightly lower, as some heat is used for heating. Similarly, the light green line represents DHW, following a similar trend. However, in the summer, the outlet temperature is slightly higher due to the lower demand for DHW heating.

The COP of the HP for the integrated system considering both SH and DHW is presented in Fig. 19, evaluated on a weekly and annual basis. The system's performance can be assessed through the COP values of the HP with PVT and ATES system. As discussed earlier, SH demand is highest during the winter months. The HP combined with PVT for SH achieves an average COP of around 5 during winter weeks (see Fig. 19(a)). In contrast, the HP combined with ATES for SH reaches a higher average COP of approximately 7 due to higher inlet temperature, though with greater variability. For DHW, when using the HP with ATES, the COP is lower, around 4, but shows consistent performance throughout. Similar trends are observed during spring weeks, although SH demand is less frequent during this period, meaning the HP is not always in use. In the summer, only DHW is required, and ATES is used with the HP to meet this demand. The COP remains steady at around 4, reflecting consistent system performance. Fig. 19(b) presents the annual COP for the different scenarios. The lowest COP is observed for DHW, as the heating demand is continuous and higher temperature is required to cover DHW demand. In contrast, SH, particularly when using a HP with ATES, achieves the highest annual COP. This is due to the system's better performance during peak demand periods, such as winter, and a lower temperature required to meet this demand. This shows that the ATES-HP combination for SH provides better performance over the course of a year, making it a suitable configuration due to the higher inflow temperature from the warm aquifer. The average annual COP of the HP in this case considering both SH and DHW is approximately 5.31.

Furthermore, Fig. 20 illustrates the power consumed by the HP to meet SH and DHW demands using thermal energy from the PVT and ATES systems, both on a weekly and annual basis. Much lower power is required during the spring weeks compared to the winter weeks, due to lower heating demand as shown in Fig. 20(a). The HP with ATES system generally consumes more power, particularly during the winter months, as it is primarily responsible for covering SH demand as illustrated in Fig. 20(b). This increased power consumption also shows greater variability due to the fluctuating heating needs in colder months. In contrast, the HP combined with the PVT system exhibits lower and more consistent power consumption throughout the year, especially for SH. For DHW, power is required year-round to meet the constant demand and the energy consumption is more stable compared to SH. Since the COP is directly related to power usage, HPs with higher COP values (such as those combined with ATES for SH) will require less power to deliver the same heating output. In contrast, HPs with lower COP values (such as those combined with ATES for DHW) will consume more power due to the higher temperature requirement to meet DHW demand compared to SH demand.

The annual temperature variations in warm and cold aquifers of the seasonal storage system is shown in Fig. 21. Considering current insulation case, volume of 20,000 $m^3$ for each aquifer is thought to be sufficient. Two distinct temperature profiles are observed: the warm aquifer, shown in red, and the cold aquifer, shown in blue. The warm aquifer temperature ranges from a minimum of 25 °C to a maximum of 26.76 °C, with a noticeable increase around mid-year due to thermal energy storage from the PVT collectors. On the other hand, the cold aquifer remains cooler, with temperatures between 13 °C and 15 °C. Both aquifers generally warm up as the year goes on, but the cold aquifer experiences a more significant rise in the temperature. Throughout the year, the temperature difference between the two aquifers remains substantial, averaging around 12 °C. The temperature fluctuations in both aquifers are less than 3 °C, indicating that the aquifer sizes are appropriate for the system.

For the weekly and annual operation of the system, the entire heating and cooling demand is covered by dividing it into five different modes, utilizing a series of switches to direct heat flow as mentioned in Section 3.2. In the considered configuration, where PVT collectors are used alongside radiator heating, the system operates in the following manner. During peak winter weeks, only mode III is activated to meet the heating demand. During spring, both modes I and II are activated in response to increased solar radiation. However, they operate only for a few hours during the day, as the PVT collectors generate heat only when sunlight is available. In contrast, during the summer weeks, both DHW and cooling are required. This activates mode IV for cooling and mode V for DHW, as shown in Fig. 22(a). The annual operation of the system is depicted in Fig. 22(b), where it can be seen that modes I, II, and III are active during the winter and spring months, while modes IV and V are primarily activated during the summer and autumn months.

To analyze the system dynamics, Fig. 23 illustrates the energy input from the warm aquifer and PVT collectors with a HP, necessary to meet the demands for SH and DHW. The energy output from the ATES combined with the HP for SH, shown by the red line, demonstrates significant seasonal fluctuations. During the winter months, the average energy supplied peaks at approximately 80 kWh per day, reflecting the high heating demand. In contrast, during the summer and autumn months, energy output drops sharply due to reduced heating needs, driven by higher ambient temperatures and increased solar irradiance.

The energy output from the PVT collectors combined with the HP, represented by the pink line, remains relatively low and stable throughout the year. There is a slight increase during the spring months, when the output occasionally peaks, likely attributed to enhanced solar irradiance. The contribution from solar collectors, indicated by the dashed green line, is minimal compared to the other configurations. However, the surplus heat

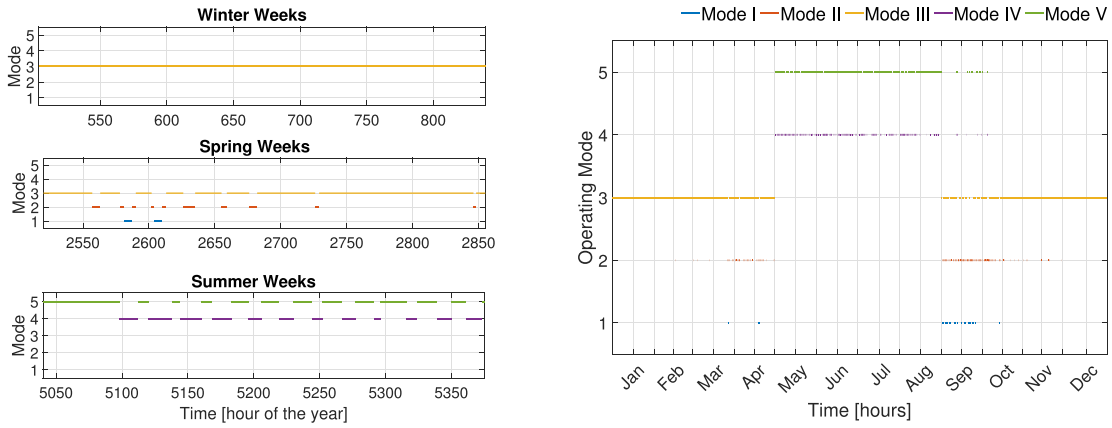


(a) Activation of modes during winter, spring and summer weeks (b) Activation of modes throughout the year

**Fig. 22.** Operational modes of the system with current insulation for SH, DHW and cooling with radiator heating for (a) weekly and (b) annual activation.

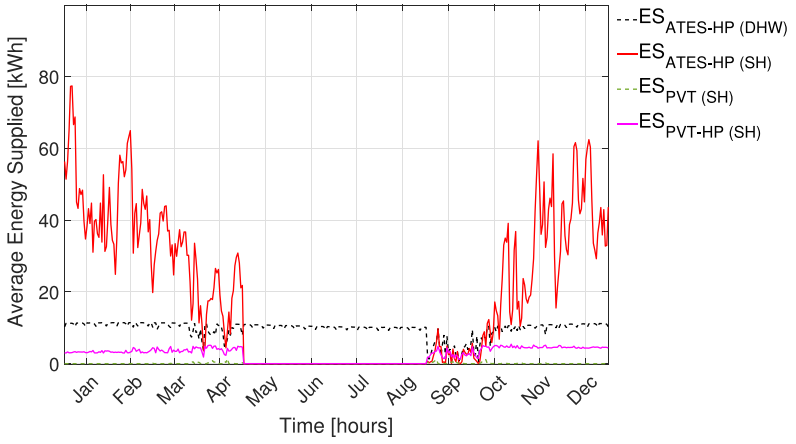


**Fig. 23.** Average energy supplied by various components to cover heating demand using current insulation. (For interpretation of the references to color in this figure legend, the reader is referred to the web version of this article.)

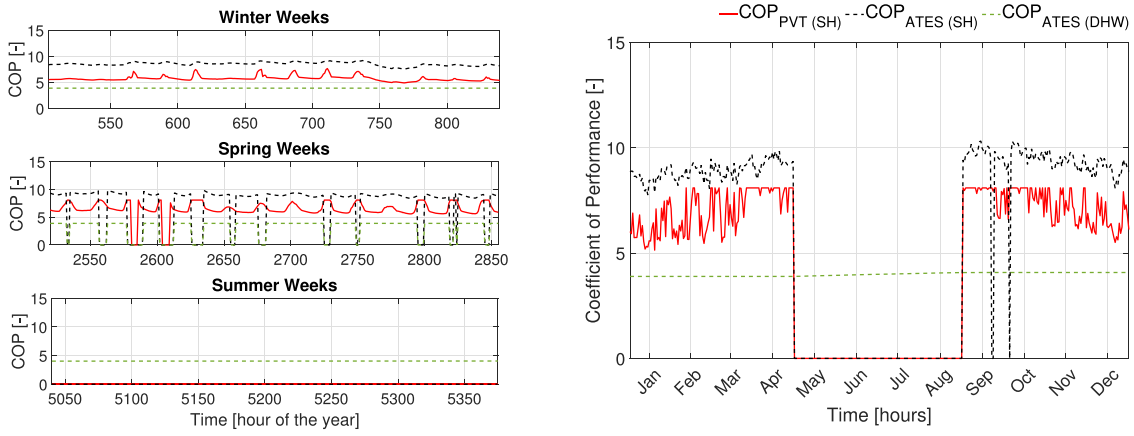


(a) Weekly variation of COP (b) Annual variation of COP

**Fig. 24.** COP of the HP with floor heating for DHW and SH, utilizing ATES and PVT systems for (a) weekly and (b) annual variation.

generated by the solar collectors during summer season is stored in the warm aquifer. The ATES in combination with the HP for DHW, illustrated by the dashed black line, maintains a steady energy output throughout the year, typically ranging from 8 to 16 kWh per day. This stability indicates a consistent demand for DHW, with only minor fluctuations around the average value. Overall, this analysis emphasizes the critical roles of each system and highlights how seasonal variations significantly affect their performance.

- **Current insulation with floor heating**

  The next section examines the use of unglazed PVT collectors, where the heating method shifts from radiator heating to floor

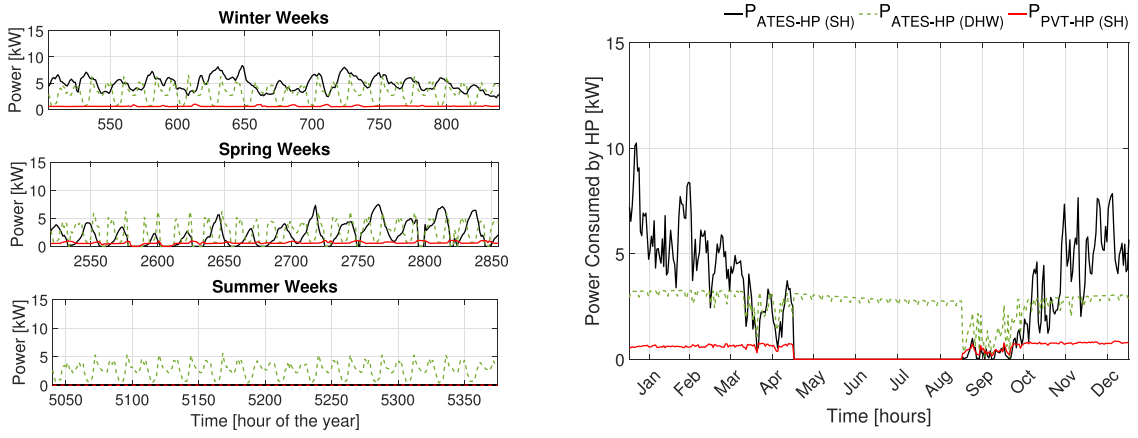


(a) Weekly variation of power

(b) Average annual variation of power

**Fig. 25.** Power consumption of the HP with floor heating for DHW and SH, utilizing ATES and PVT systems for (a) weekly and (b) average annual variation.

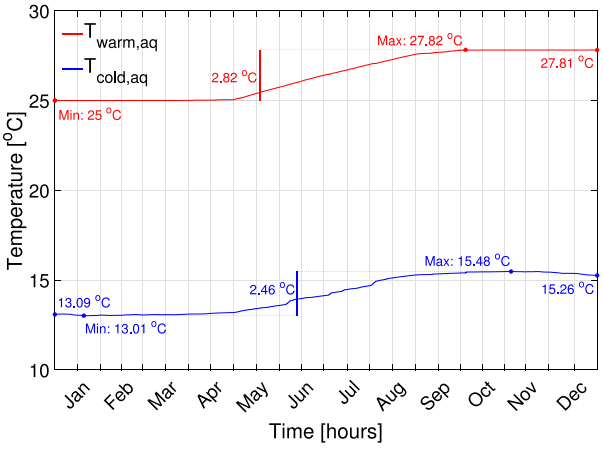


**Fig. 26.** Annual temperature variation with $T_M$-level insulation of the aquifers considering PVT collectors and radiator heating, highlighting their seasonal fluctuations.

heating, which requires lower temperatures to meet the SH demand. Fig. 24 illustrates that the COP for DHW using a HP with the ATES remains consistent with that of radiator heating. However, there is a notable increase in the COP for both heating scenarios. In the radiator heating configuration, the combination of PVT collectors and the HP achieves an average COP of approximately 5 during winter weeks. In contrast, with the floor heating system, the COP rises to around 6. This improvement is due to the lower temperature required for floor heating compared to radiator heating. Furthermore, the HP combined with ATES for SH reaches an average COP of approximately 7 in the previous case, while in this scenario, it exceeds 8. Overall, the average annual COP for both SH and DHW in this configuration is approximately 5.87. This improvement demonstrates the effectiveness of floor heating systems in enhancing energy efficiency. The higher COP values reflect the system's ability to provide heating more efficiently, highlighting the benefits of selecting appropriate heating method for optimal performance.

Fig. 25 depicts the power consumption of the HP to meet SH and DHW demands utilizing floor heating, both on a weekly and on annual basis. In floor heating case, the power consumed by the HP for SH has decreased significantly compared to the previous radiator heating configuration. This reduction is largely due to the lower temperature requirements of the floor heating system, which enhances the COP of the HP. With an increased COP of approximately 6 for SH, the system requires less power to deliver the same heating output. Consequently, this results in lower energy consumption, especially during the colder months, while still maintaining the ability to meet heating demands effectively. The more efficient operation of the floor heating system not only reduces power requirements but also contributes to overall system performance.

- **$T_M$ and $T_L$ level insulation with radiator heating**

  As explained earlier, the use of $T_M$-level insulation reduces the annual heating demand from 194 MWh to 95 MWh for all the considered buildings (see Fig. 12(a)). This results in a smaller required aquifer volume, which is assumed 14,000 $m^3$ approximately for each aquifer as the temperature fluctuations in each aquifer are less than 3 °C. The number of solar collectors reduced to 60% of the previous amount because of the lower demand. With the use of PVT collectors and radiator heating, the cold aquifer end temperature remains nearly the same at 15.26 °C, compared to 15.18 °C with the current insulation, as shown in Fig. 26. However, the warm aquifer temperature increases to 27.81 °C, up from 26.76 °C with the current insulation. This indicates that the new insulation reduces the SH demand and leads to a lessened extraction of heat, causing the warm aquifer temperature to rise. Meanwhile, the cooling demand remains largely unaffected by the change in insulation, so the cold aquifer temperature stays approximately the same.

  Considering the similar case with $T_M$-level insulation, the operating modes for both winter and summer weeks remain consistent, as shown in Fig. 27(a). However, it is interesting to note the use of operating modes IV and V during the spring months. Mode IV, that is for cooling, experiences slight changes in the demand due to the building's insulation, with some spikes observed. On the other hand, mode V is activated on several occasions to cover DHW demand. The reason for this is that SH demand is reduced and is not much required during spring weeks whereas DHW remains the same as previous case. Also the warm aquifer temperature in this case is a bit higher compared to the previous case.

  Additionally, the average annual COP for both SH and DHW in the previous case was approximately 5.31. However, with the new insulation, the COP decreases to 5.05, as less SH is required while the demand for DHW remains unchanged. A similar trend was observed across all cases, regardless of the heating type or collector used. During the winter months, the average energy supplied peaks at approximately 45 kWh per day with $T_M$-level

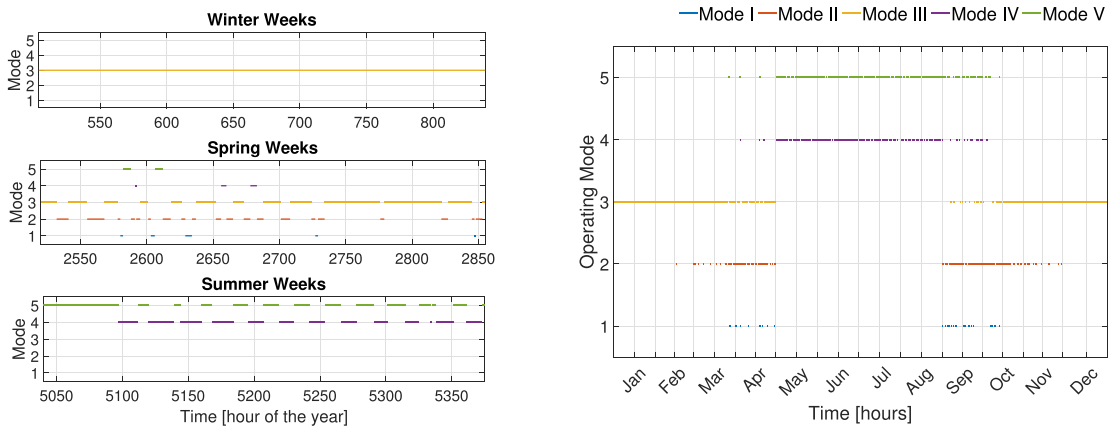


(a) Activation of modes during winter, spring and summer weeks (b) Activation of modes throughout the year

**Fig. 27.** Operational modes of the system with $T_M$-level insulation for SH, DHW and cooling with radiator heating for (a) weekly and (b) annual activation.

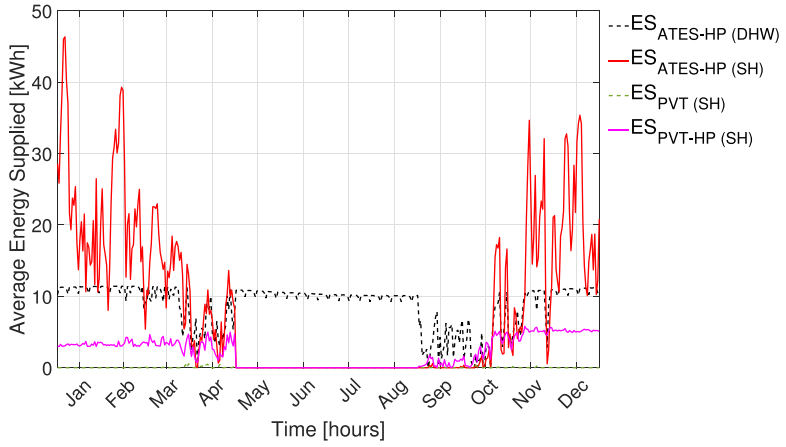


**Fig. 28.** Average energy supplied by various components to cover heating demand using $T_M$-level insulation.

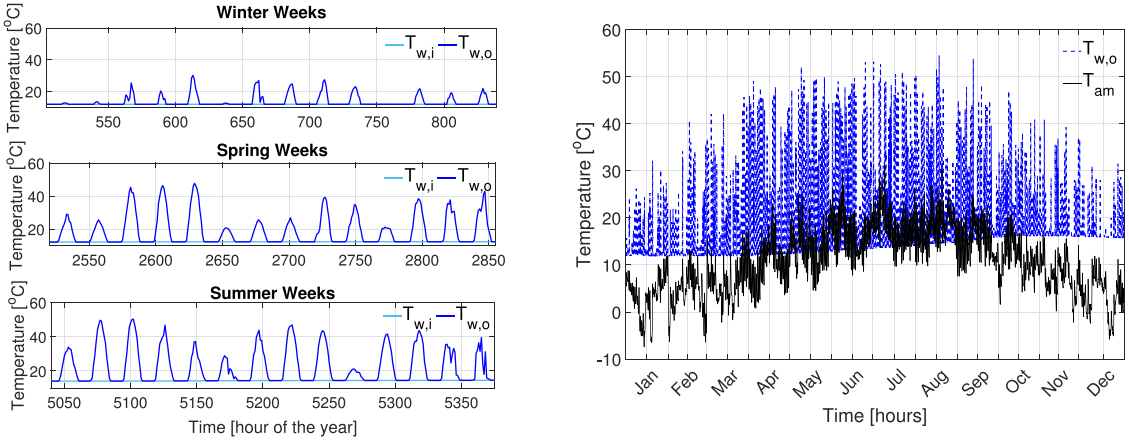


(a) Weekly variation of temperatures (b) Annual variation of temperatures

**Fig. 29.** Variation of inflow and outflow temperatures considering ST collectors and radiator heating for (a) weekly and (b) annual variation.

insulation as illustrated in Fig. 28, compared to 80 kWh per day, reflecting a lower SH demand. Similar to the previous case, during the summer and autumn months, the energy output drops sharply due to reduced heating needs. However, since the DHW demand is unaffected by the change in insulation, a similar trend in energy usage for DHW can be observed, maintaining consistent energy supply throughout the seasons.

Lastly, with $T_L$-level insulation, the SH demand is further reduced to 50 MWh. This implies the aquifer size can be further minimized. However, it is important to note that the DHW demand

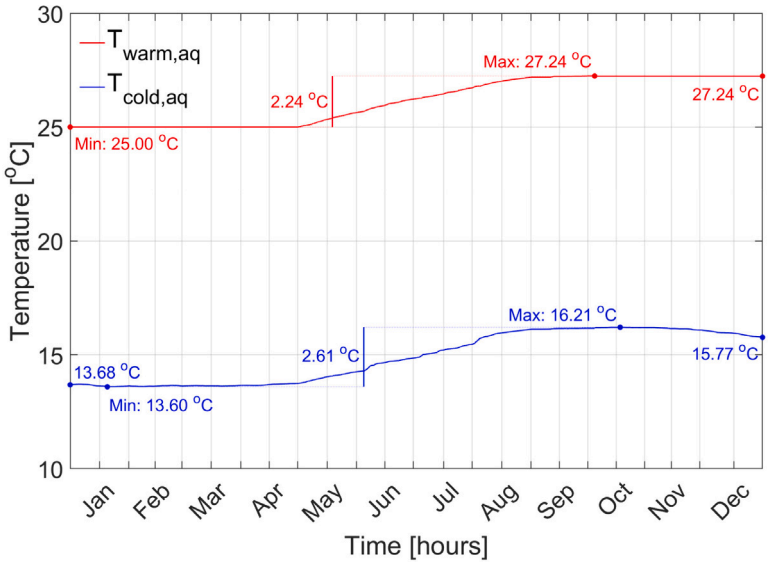


**Fig. 30.** Annual temperature variation of the aquifers considering ST collectors and radiator heating, highlighting their seasonal fluctuations.

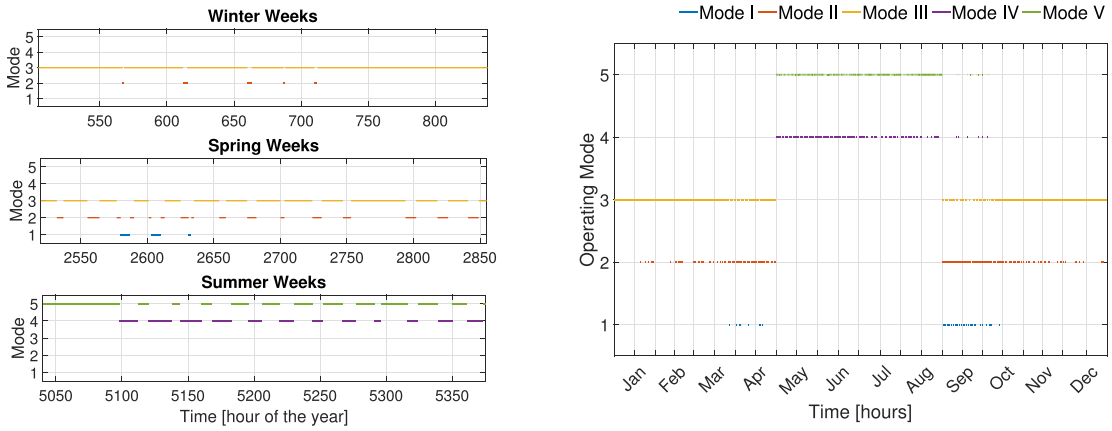


(a) Activation of modes during winter, spring and summer weeks (b) Activation of modes throughout the year

**Fig. 31.** Operational modes of the system for SH, DHW and cooling with radiator heating for (a) weekly and (b) annual variation.

remains constant at approximately 92.70 MWh, as it is unaffected by insulation. If a similar aquifer size is maintained as in the previous case with $T_L$-level insulation, the cold aquifer remains unchanged. However, the temperature of the warm aquifer increases slightly to 27.92 °C due to reduced heat extraction for SH. As a result of the reduced SH demand, the combined COP decreases to 4.88 which was 5.31 with current and 5.05 with the $T_M$-level insulation.

- **$T_M$ and $T_L$ level insulation with floor heating**
  In this configuration, radiator heating is replaced by floor heating, while maintaining the new level of insulation. The use of floor heating increases the COP of the HP for the integrated system to 5.43, compared to 5.05 in the previous case. However, the COP remains lower when compared to the current insulation level, which was 5.87 in the case of floor heating. Additionally, the aquifers temperature remains approximately the same as in the case of radiator heating with the new insulation levels.

*5.2.2. Case B: PV/ST collectors*

In this case, the PVT collectors are replaced with separate ST and PV modules. While unglazed PVTs were used in the previous scenario, this configuration uses glazed ST collectors for heat production. This results in reduced heat losses to the ambient environment and higher outlet temperatures.

- **Current insulation with radiator heating**
  In this part, radiator heating is utilized with current insulation. Although this setup requires more roof space for the two modules, Fig. 29 shows that ST collector temperatures often exceed 50 °C, compared to 40 °C from unglazed PVT collectors. Notably, the glazed ST collectors maintain high temperatures not only during the summer months but also during winter. This indicates increased heat storage in the warm aquifer, increasing the utilization of modes I and II. Weekly temperature variations across multiple seasons are depicted in Fig. 29(a), while annual temperature variations are illustrated in Fig. 29(b).
  The difference in aquifer temperature can be observed in Fig. 30 when using glazed ST collectors. With the same aquifer volume, the final temperature of the warm aquifer is 27.24 °C, showing a noticeable increase from the previous case, where it was 26.76 °C. In contrast, the cold aquifer reaches a temperature of 15.77 °C, compared to just above 15 °C in the earlier scenario. Both aquifers warm as the year progresses, with temperature fluctuations under 3 °C, indicating their sizes are suitable for the system. Throughout

the year, the temperature difference between the two aquifers remains substantial, averaging around 12 °C, which is significant. Given the higher temperatures achieved, it may be possible to reduce the number of ST collectors without compromising performance. The average annual COP for both SH and DHW in this case is approximately 5.45. This shows an improvement over the previous case using PVT collectors, which had a COP of 5.31. The higher COP for the HP utilizing ST collectors indicates better energy efficiency, demonstrating the enhanced performance of ST collectors in converting solar energy into useful heating.

In the Netherlands, electricity supply exceeds the demand, especially during peak production (sunshine hours) in the summer months. Instead of shutting the PV modules or causing strain on the grid, excess electricity from the PV modules can be utilize to operate the HP. By converting excess electricity into heat and store it to the seasonal storage, the system avoids sending surplus power to the grid during peak production times. In this case, the excess electricity produced is approximately 1168 kWh when heating is not required. The HP operates with a COP of 4 since cold aquifer fluid is utilized as an input. Utilizing PV modules and a HP, the warm aquifer temperature rises from 27.24 °C to 27.45 °C. This increase in temperature helps to enhance the COP of a HP when heating is required. The heat stored in the warm aquifer during summer can be retrieved in winter, balancing energy supply and demand. This approach can also be applied to Case A by integrating the PVT collector's PV module with the HP, enabling surplus electricity to be converted into heat and stored in seasonal storage.

- **Current insulation with floor heating**
  In this configuration, not only are the PVT collectors replaced with separate ST and PV modules, but the heating system is shifted from radiator heating to floor heating. The use of ST collectors allows for more heat to be stored in the warm aquifer, leading to an increased utilization of the first two modes (I and II) of operation. Additionally, the lower temperature requirements of floor heating further enhance system performance. During the winter weeks in the previous configuration where PVTs and radiator heating were used, only mode III was activated. However, in this case as shown in Fig. 31(a), mode II also gets activated during certain hours, reflecting improvement in the system. During the spring weeks, not only do the activation hours for mode I increase. Mode II also becomes more active, further optimizing energy utilization by taking advantage of the lower temperature demands of the floor heating system. This results in better system performance throughout the year, with more modes engaged to efficiently meet heating demands. In this configuration, the HP achieves an average COP of 6.09 for both SH and DHW, marking a significant improvement over previous configurations. This increase is driven by the combined benefits of using separate ST modules, along with the switch to floor heating. The ST collectors allow for more efficient heat storage in the warm aquifer, while the lower temperature requirements of floor heating reduce the load on HP, enhancing its COP. As a result, the system can deliver the same heating output with less energy input, leading to a higher overall COP of the HP. This improvement highlights how changes in configuration, such as optimizing heat sources and distribution methods, can substantially boost performance.
- **$T_M$ and $T_L$ level insulation with radiator heating**
  The implementation of $T_M$-level insulation reduces the annual heating demand, leading to a smaller required aquifer volume and fewer collectors. However, with the combination of PV/ST collectors, the warm aquifer's temperature rises to approximately 28 °C due to the additional heat provided by the ST collectors. Moreover, the inclusion of ST collectors increases the COP of the HP for both SH and DHW to 5.16, compared to 5.05 in the case of PVT usage with the same configuration.
- **$T_M$ and $T_L$ level insulation with floor heating**
  A similar trend was observed here as was noted in Case A, where PVTs were utilized with a similar configuration.

## 6. Conclusions

The present effort focuses on five residential buildings in Amsterdam. Different types of solar collectors combined with seasonal storage and HP have been studied and numerous modes are compared considering radiator and floor heating. The main findings of this study are summarized as follow:

- Unglazed PVT collectors achieve a 7.70% higher electrical output than standalone PV modules by reducing cell temperature through heat extraction, simultaneously delivering usable thermal energy.
- Glazed ST collectors achieve about 70% higher thermal performance than unglazed PVT collectors due to better heat retention and lower losses. Considering Dutch climate, glazed ST consistently exceed 50 °C, while PVT collectors peak at 40 °C.
- Solar collectors with HPs for SH achieve an average COP of 5, while seasonal storage with HPs reaches about 7, due to higher input temperatures. Additionally, HPs with higher COP values, like those combined with seasonal storage for SH, use less power for the same heating output, while those with lower COP values for DHW consume more due to higher temperature demands.
- A PV/ST system with floor heating achieves a higher COP of 6.09 compared to 5 for radiator heating with PVTs, due to lower temperature needs. Moreover, ST collectors with floor heating activate more modes in winter and spring to better meet heating demand.
- Across all cases, most energy is supplied by seasonal storage with a HP. Mode III meets most heating demand, while Mode I, though supplying less, is crucial for storing heat in the warm aquifer during summer.
- The warm aquifer temperature increases with the new insulation due to lower SH demand and lessened heat extraction. Additionally, the enhancement in insulation reduces the overall COP for all the considered cases.

In conclusion, regarding heat production and heat storage, utilizing PV/ST combination and floor heating is an effective solution for meeting energy demands. This combination outperforms PVT-based systems as activation hours for different modes are increased, the HP achieves a better COP and higher temperatures can be observed in the warm aquifer. However, PV/ST configuration requires a larger roof area as separate PV and ST modules are utilized.

The model developed in this work will be used in future work to further investigate the following:

- Assess the performance and economic analysis of the integrated system in various climates, including southern European countries, to evaluate its adaptability.
- Explore the use of high-temperature ATES systems and consider thermal stratification.
- Investigate the use of surplus PV electricity in the Netherlands during summer to operate heat pumps for storing thermal energy for winter use.
- Conduct experimental validation to further confirm the accuracy and enhance the reliability of the results.

Taking all the results into consideration, it can be concluded that the integrated system considering multiple modes and scenarios possess a significant potential to cover heating and cooling demands of the buildings.

## CRediT authorship contribution statement

**Zain Ul-Abdin:** Writing – review & editing, Writing – original draft, Methodology, Investigation, Data curation, Conceptualization. **Olindo Isabella:** Writing – review & editing, Project administration, Funding acquisition. **Rudi Santbergen:** Writing – review & editing, Supervision, Conceptualization.

## Declaration of competing interest

The authors declare that they have no known competing financial interests or personal relationships that could have appeared to influence the work reported in this paper.

## Acknowledgments

This project has been developed in the framework of the PED Program, which is implemented by the Joint Programming Initiative Urban Europe and SET Plan Action 3.2. The Austrian part is supported by the Austrian Ministry of Climate Action, Environment, Energy, Mobility, Innovation, and Technology (BMK), The Netherlands; the Romanian part is supported by a grant of the Ministry of Research, Innovation and Digitization CNCS/CCCDI – UEFISCDI, The Netherlands, project number PED-JPI-SIMPLY POSITIVE, contracts number 325/2022 and 326/2022, within PNCDI III; the Dutch part is supported by the RVO, The Netherlands (the Netherlands Enterprise Agency), reference number ERANETPED-02767306; and the Italian part is supported by a grant of the Ministry of Education and Merit - Department for Higher Education and Research, The Netherlands, project number PED_00042, from the Fund for Investment in Scientific and Technological Research (FIRST/FAR), The Netherlands and/or Special Accounting Account no. 5944.

The authors extend their gratitude to Dr. Maeva Dang and Paul Voskuilen from AMS Institute for providing the heat demand profiles of various residential buildings, which served as a vital foundation for this study. We would also like to express our sincere gratitude to David E. Martinez Aguilera and Divye Nikhil Kanawala, former MSc students at TU Delft, for their valuable contributions to this research. Their assistance in data collection was instrumental in completing this work.

## References

[1] Q. Hassan, P. Viktor, T.J. Al-Musawi, B.M. Ali, S. Algburi, H.M. Alzoubi, A.K. Al-Jiboory, A.Z. Sameen, H.M. Salman, M. Jaszczur, The renewable energy role in the global energy transformations, Renew. Energy Focus. 48 (2024) 100545.
[2] Ember, European electricity review 2025, 2025, https://ember-energy.org/latest-insights/european-electricity-review-2025/. (Accessed 10 February 2025).
[3] A. Ahmed, T. Ge, J. Peng, W.-C. Yan, B.T. Tee, S. You, Assessment of the renewable energy generation towards net-zero energy buildings: A review, Energy Build. 256 (2022) 111755.
[4] E. Ohene, A.P. Chan, A. Darko, Review of global research advances towards net-zero emissions buildings, Energy Build. 266 (2022) 112142.
[5] M. Dehghan, S. Rahgozar, A. Pourrajabian, M. Aminy, F.-S. Halek, Techno-economic perspectives of the temperature management of photovoltaic (pv) power plants: A case-study in Iran, Sustain. Energy Technol. Assess. 45 (2021) 101133.
[6] Z.B. Seddik, M. Mahdaoui, H. Makroum, M. Ahachad, 4E performance evaluation of pv, pv/thermal, and solar domestic water heater for building integration in the Moroccan country, Energy Convers. Manage. 272 (2022) 116380.
[7] A.K. Pandey, R. Kumar, M. Samykano, Solar energy: direct and indirect methods to harvest usable energy, in: Dye-Sensitized Solar Cells, Elsevier, 2022, pp. 1–24.
[8] S. Ying, X. Zhang, Y. Wu, Z. Pan, Solar photovoltaic/thermal (pv/t) systems with/without phase change materials (pcms): A review, J. Energy Storage 89 (2024) 111582.
[9] J.F. Rosales-Pérez, A. Villarruel-Jaramillo, J.A. Romero-Ramos, M. Pérez-García, J.M. Cardemil, R. Escobar, Hybrid system of photovoltaic and solar thermal technologies for industrial process heat, Energies 16 (5) (2023) 2220.
[10] H. Fares, N. Le Pierrès, D. Cheze, E. Wurtz, Assessing the energy performance of solar photovoltaic, thermal and hybrid pvt panels in a building context: A systematic study of the criteria'definitions and studies parameters, Sol. Energy 286 (2025) 113126.
[11] A.M. Alshibil, I. Farkas, P. Víg, Multi-aspect approach of electrical and thermal performance evaluation for hybrid photovoltaic/thermal solar collector using trnsys tool, Int. J. Thermofluids 16 (2022) 100222.
[12] H. Bruckner, S. Alyokhina, S. Schneider, M. Binder, Z.U. Abdin, R. Santbergen, M. Verkou, M. Zeman, O. Isabella, M. Pagliarini, et al., Lessons learned from four real-life case studies: Energy balance calculations for implementing positive energy districts, Energies 18 (3) (2025) 1–17.
[13] Y. Zhang, J. Ji, Z. Song, W. Ke, H. Xie, Performance prediction on a novel dual-mode heat pump with a hybrid photovoltaic/micro-channel heat pipe/fin heat exchanger, Energy Convers. Manage. 293 (2023) 117505.
[14] T. You, W. Wu, H. Yang, J. Liu, X. Li, Hybrid photovoltaic/thermal and ground source heat pump: Review and perspective, Renew. Sustain. Energy Rev. 151 (2021) 111569.
[15] E. van der Roest, S. Beernink, N. Hartog, J.P. van der Hoek, M. Bloemendal, Towards sustainable heat supply with decentralized multi-energy systems by integration of subsurface seasonal heat storage, Energies 14 (23) (2021) 7958.
[16] M. Bloemendal, T. Olsthoorn, F. van de Ven, Combining climatic and geo-hydrological preconditions as a method to determine world potential for aquifer thermal energy storage, Sci. Total Environ. 538 (2015) 621–633.
[17] S. Beernink, N. Hartog, P.J. Vardon, M. Bloemendal, Heat losses in ates systems: The impact of processes, storage geometry and temperature, Geothermics 117 (2024) 102889.
[18] J. Waluyo, R.D.D. Putra, D.C. Adhitya, R.A. Rahman, Parametric operational analysis of hybrid thermo-electric/fluid-active thermal storage for domestic water heating system, Sol. Energy Mater. Sol. Cells 286 (2025) 113575.
[19] Y. Liang, D. Wang, Y. Li, Q. Zhang, B. Suolang, X. Yuan, Y. Liu, Novel approach to remote rural heating: Direct coupled photovoltaic electric heater underfloor heating system with phase change materials, Appl. Therm. Eng. 250 (2024) 123525.
[20] D.S. Yuseva, R. Anggrainy, R.D.D. Putra, R.A. Rahman, Performance evaluation of combined passive/active thermal charge/discharge latent heat tank with stabilized-solid–Liquid storage material for intermediate thermal storage system, Int. J. Thermofluids 23 (2024) 100732.
[21] C. Zhang, Z. Jiao, J. Liu, K. Ning, Robust planning and economic analysis of park-level integrated energy system considering photovoltaic/thermal equipment, Appl. Energy 348 (2023) 121538.
[22] TGVillage, Go-sun, returning solar heat to the heating network, 2024, https://www.thegreenvillage.org/project/go-zon/. (Accessed 12 April 2024).
[23] A. Del Amo, A. Martínez-Gracia, A.A. Bayod-Rújula, M. Cañada, Performance analysis and experimental validation of a solar-assisted heat pump fed by photovoltaic-thermal collectors, Energy 169 (2019) 1214–1223.
[24] J. Clauß, L. Georges, Model complexity of heat pump systems to investigate the building energy flexibility and guidelines for model implementation, Appl. Energy 255 (2019) 113847.
[25] M. Aldubyan, A. Chiasson, Thermal study of hybrid photovoltaic-thermal (pvt) solar collectors combined with borehole thermal energy storage systems, Energy Procedia 141 (2017) 102–108.
[26] A. Perera, K. Soga, Y. Xu, P.S. Nico, T. Hong, Enhancing flexibility for climate change using seasonal energy storage (aquifer thermal energy storage) in distributed energy systems, Appl. Energy 340 (2023) 120957.
[27] H. Ghaebi, M. Bahadori, M. Saidi, Performance analysis and parametric study of thermal energy storage in an aquifer coupled with a heat pump and solar collectors, for a residential complex in Tehran, Iran, Appl. Therm. Eng. 62 (1) (2014) 156–170.
[28] P. Fleuchaus, S. Schüppler, B. Godschalk, G. Bakema, P. Blum, Performance analysis of aquifer thermal energy storage (ates), Renew. Energy 146 (2020) 1536–1548.
[29] Deltares, Deltares: Aquifer thermal energy storage, 2024, https://www.deltares.nl/en/expertise/areas-of-expertise/energy-transition/aquifer-thermal-energy-storage. (Accessed 15 April 2025).
[30] M. Vogt, C.R. Tobon, A. Alcaniz, P. Procel, Y. Blom, A.N. El Din, T. Stark, Z. Wang, E.G. Goma, J. Etxebarria, et al., Introducing a comprehensive physics-based modelling framework for tandem and other pv systems, Sol. Energy Mater. Sol. Cells 247 (2022) 111944.
[31] Z. Ul-Abdin, M. Zeman, O. Isabella, R. Santbergen, Investigating the annual performance of air-based collectors and novel bi-fluid based pv-thermal system, Sol. Energy 276 (2024) 112687.
[32] M.E.A. Slimani, M. Amirat, I. Kurucz, S. Bahria, A. Hamidat, W.B. Chaouch, A detailed thermal-electrical model of three photovoltaic/thermal (pv/t) hybrid air collectors and photovoltaic (pv) module: Comparative study under algiers climatic conditions, Energy Convers. Manage. 133 (2017) 458–476.
[33] C. Shen, Y. Zhang, C. Zhang, J. Pu, S. Wei, Y. Dong, A numerical investigation on optimization of pv/t systems with the field synergy theory, Appl. Therm. Eng. 185 (2021) 116381.
[34] B. Lamrani, A. Draoui, F. Kuznik, Thermal performance and environmental assessment of a hybrid solar-electrical wood dryer integrated with photovoltaic/thermal air collector and heat recovery system, Sol. Energy 221 (2021) 60–74.
[35] M. Mortadi, A. El Fadar, O.A. Begdouri, 4E analysis of photovoltaic thermal collector-based tri-generation system with adsorption cooling: Annual simulation under moroccan climate conditions, Renew. Energy 221 (2024) 119828.

[36] VDMA, International technology roadmap for photovoltaics (itrpv), 2024.
[37] Y.W. Koholé, F.C.V. Fohagui, G. Tchuen, Flat-plate solar collector thermal performance assessment via energy, exergy and irreversibility analysis, Energy Convers. Manag. 15 (2022) 100247.
[38] Z. Ul Abdin, A. Rachid, Bond graph modeling of a water-based photovoltaic thermal (pv/t) collector, Sol. Energy 220 (2021) 571–577.
[39] Z.M. Mahdi, A.N. Al-Shamani, A. Al-Manea, H.A. Al-zurfi, R. Al-Rbaihat, K. Sopian, A. Alahmer, Enhancing photovoltaic thermal (pvt) performance with hybrid solar collector using phase change material, porous media, and nanofluid, Sol. Energy 283 (2024) 112983.
[40] Huntkey, Huntkey: The most comprehensive guide to thermal energy storage, 2024, https://www.huntkeyenergystorage.com/thermal-energy-storage/. (Accessed 14 April 2025).
[41] C. Doughty, G. Hellström, C.F. Tsang, J. Claesson, A dimensionless parameter approach to the thermal behavior of an aquifer thermal energy storage system, Water Resour. Res. 18 (3) (1982) 571–587.
[42] M. Bloemendal, N. Hartog, Analysis of the impact of storage conditions on the thermal recovery efficiency of low-temperature ates systems, Geothermics 71 (2018) 306–319.
[43] V. Silvestri, G. Crosta, A. Previati, P. Frattini, M. Bloemendal, Uni-directional ates in high groundwater flow aquifers, Geothermics 125 (2025) 103152.
[44] Divye Nikhil Kanawala, Optimization of heating and cooling systems consisting of PVT collectors, seasonal storage and heat pumps (Master's thesis), Delft University of Technology, Netherlands, 2024.
[45] M. Diederen, Assessment of the Impact of Ambient Groundwater Flow on High Temperature Aquifer Thermal Energy Storage (Ht-Ates) Performance and Thermal Spreading (Master's thesis), 2019.
[46] W. Sommer, Modelling and Monitoring of Aquifer Thermal Energy Storage : Impacts of Soil Heterogeneity, Thermal Interference and Bioremediation (WU thesis), Internal Phd, Wu, Wageningen University, Netherlands, 2015, p. 6052.
[47] J. Ward, C. Simmons, P. Dillon, A theoretical analysis of mixed convection in aquifer storage and recovery: How important are density effects? J. Hydrol. 343 (2007) 169–186.
[48] F. Fossoul, P. Orban, A. Dassargues, Numerical simulation of heat transfer associated with low enthalpy geothermal pumping in an alluvial aquifer, Geol. Belg. 14 (1–2) (2011) 45–54.
[49] R. Duijff, M. Bloemendal, M. Bakker, Interaction effects between aquifer thermal energy storage systems, Groundw. 61 (2021).
[50] D.M. Aguilera, Integration and Optimization of a Solar Collector Heat Pump System Model for Households in the Netherlands (Master's thesis), Delft University of Technology, Netherlands, 2024.
[51] O. Ruhnau, L. Hirth, A. Praktiknjo, Time series of heat demand and heat pump efficiency for energy system modeling, Sci. Data 6 (1) (2019) 1–10.
[52] S. Chaturvedi, V. Gagrani, T. Abdel-Salam, Solar-assisted heat pump–A sustainable system for low-temperature water heating applications, Energy Convers. Manage. 77 (2014) 550–557.
[53] M. Barbu, M. Siroux, G. Darie, Numerical model and parametric analysis of a liquid based hybrid photovoltaic thermal (pvt) collector, Energy Rep. 7 (2021) 7977–7988.
[54] W.N.A.W. Roshdan, H. Jarimi, A.H. Al-Waeli, O. Ramadan, K. Sopian, Performance enhancement of double pass photovoltaic/thermal solar collector using asymmetric compound parabolic concentrator (pv/t-acpc) for façade application in different climates, Case Stud. Therm. Eng. 34 (2022) 101998.
[55] M. Hakimi, E. Baniasadi, E. Afshari, A comparative study on novel active cooling and heat recovery techniques for photovoltaic-thermal collectors, Process. Saf. Environ. Prot. 190 (2024) 1233–1252.
[56] D. Wu, B. Ma, X. Huang, X. Wu, Y. Yang, C. Wen, J. Zhang, Heat exchanger design and performance evaluation for a high-temperature heat pump system under different two-phase correlations: 4e analysis, Appl. Energy 384 (2025).
[57] A. van Rossum, Developing and Implementing Toolbox Integrations for Storing Excess Heat Generated By a Pvt System (Master's thesis), 2024.
[58] H. Paksoy, Z. Gürbüz, B. Turgut, D. Dikici, H. Evliya, Aquifer thermal storage (ates) for air-conditioning of a supermarket in Turkey, Renew. Energy 29 (12) (2004) 1991–1996.
[59] Rvonl, Voorbeeldwoningen bestaande bouw, 2022, https://www.rvo.nl/sites/default/files/2023-01/brochure-voorbeeldwoningen-bestaande-bouw-2022.pdf. (Accessed 26 April 2025).
[60] C. Duin, T. Koelemij, Transitievisie warmte amsterdam, 2020, https://openresearch.amsterdam/nl/page/63522/transitievisie-warmte-amsterdam. (Accessed 26 April 2025).
[61] R.J. van Egmond, D. van Petersen, Tki urban energy - Kennisdossier: Warmtenetten, 2020, https://topsectorenergie.nl/nl/kennisbank/kennisdossier-warmtenetten/. (Accessed 26 Aprill 2025).
[62] J. Remund, S. Müller, M. Schmutz, P. Graf, Meteonorm version 7.3. METEOTEST, 2020, www.meteotest.com.